Department of Applied Physics

From quantum metrology to applications

Emma Mykkänen

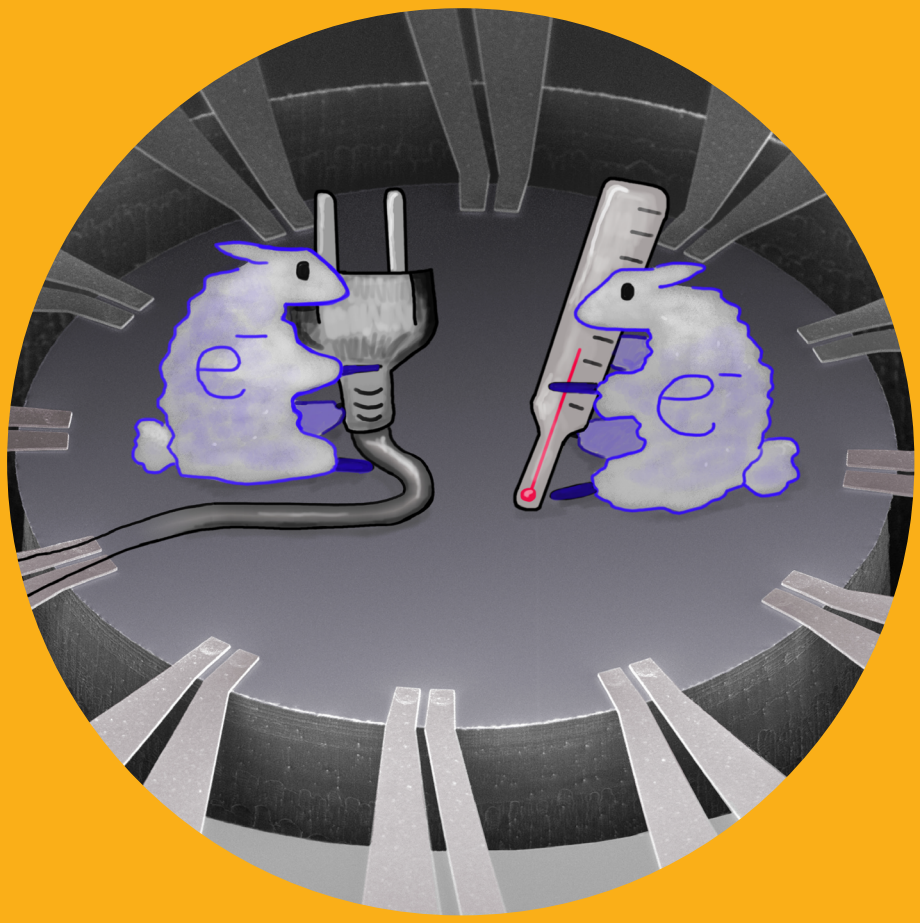

Aalto University

DOCTORAL DISSERTATIONS

Aalto University publication series
DOCTORAL DISSERTATIONS 216/2018

From quantum metrology to applications

Emma Mykkänen

A doctoral dissertation completed for the degree of Doctor of Science (Technology) to be defended, with the permission of the Aalto University School of Science, at a public examination held at the lecture hall T2 (Konemiehentie 2) of the school on 30th November 2018 at noon.

Aalto University
School of Science
Department of Applied Physics

Supervising professor
Prof. Jukka Pekola, Aalto University

Thesis advisor
Dr. Antti Kemppinen, VTT Technical Research Centre of Finland Ltd

Preliminary examiners
Prof. Ilari Maasilta, University of Jyväskylä
Dr. Frank Hohls, Physikalisch-Technische Bundesanstalt, Germany

Opponent
Prof. Alexander Tzalenchuk, National Physical Laboratory/Royal Holloway University of London, United Kingdom

Aalto University publication series
DOCTORAL DISSERTATIONS 216/2018

ISBN 978-952-60-8275-2 (printed)
ISBN 978-952-60-8276-9 (pdf)
ISSN 1799-4934 (printed)
ISSN 1799-4942 (pdf)
http://urn.fi/URN:ISBN:978-952-60-8276-9

Unigrafia Oy
Helsinki 2018

Finland

441 697
Printed matter

Aalto University

Abstract

Aalto University, P.O. Box 11000, FI-00076 Aalto www.aalto.fi

Author
Emma Mykkänen

Name of the doctoral dissertation
From quantum metrology to applications

Publisher School of Science

Unit Department of Applied Physics

Series Aalto University publication series DOCTORAL DISSERTATIONS 216/2018

Field of research Low temperature physics

Manuscript submitted 24 August 2018 **Date of the defence** 30 November 2018

Permission to publish granted (date) 12 October 2018 **Language** English

☐ **Monograph** ☒ **Article dissertation** ☐ **Essay dissertation**

Abstract

It is important that measurements produce predictable and reproducible results irrespective of time and location. This is enabled by the International System of Units (SI), which is realized through primary standards: devices that can either measure or produce a known value of a quantity without calibration against any other standard for quantity of the same kind. This thesis explores quantum standards for the ampere and the kelvin, and devices that are byproducts of this research or enablers for the devices spawning from it.

Coulomb blockade thermometer (CBT) was investigated as a possible realization of the kelvin at low temperatures. We constructed a setup, where temperature could be determined through Boltzmann constant and traceable voltage measurements. The CBT was also compared to the PLTS-2000 temperature scale and to two other Boltzmann constant based primary thermometers.

Two different quantum phenomena were studied in the context of the ampere: single-electron tunneling in superconductor -- insulator -- normal metal (NIS) junctions and quantum phase slips (QPS) in superconducting nanowires. We observed QPS in novel material: molybdenium silicide (MoSi). It has been theoretically predicted that high normal state resistivity would be beneficial for the QPS based current standard. This resistivity can be achieved in MoSi.

Since the novel standards for the ampere would produce relatively small currents (up to nanoampere), low frequency noise can increase the measurement times from hours to weeks. On the other hand, high frequency noise can initiate unwanted tunnelings and degrade the accuracy of devices. The low frequency noise problems were tackled by proper cabling and two filters were characterized in the high frequency range by NIS based detectors.

Finally we utilized the understanding of NIS systems, based on research aiming at realization of the quantum current standard, in two other applications: noise detectors and coolers. We demonstrated NIS-based cooling of a mm-scale object by silicon-aluminium junctions. The cooling was enabled by phonon transmission bottleneck. We also analyzed by simulations that electric cooling from 1.5 K to 100 mK is a realistic goal.

Keywords quantum physics, metrology, tunnel junctions, quantum standards, kelvin, ampere, electric cooling, noise filtering and detection, single-electron transport

ISBN (printed) 978-952-60-8275-2 **ISBN (pdf)** 978-952-60-8276-9

ISSN (printed) 1799-4934 **ISSN (pdf)** 1799-4942

Location of publisher Helsinki **Location of printing** Helsinki **Year** 2018

Pages 153 **urn** http://urn.fi/URN:ISBN:978-952-60-8276-9

Tekijä
Emma Mykkänen

Väitöskirjan nimi
Kvanttimittatekniikasta sovelluksiin

Julkaisija Perustieteiden korkeakoulu

Yksikkö Teknillisen fysiikan laitos

Sarja Aalto University publication series DOCTORAL DISSERTATIONS 216/2018

Tutkimusala Matalan lämpötilan fysiikka

Käsikirjoituksen pvm 24.08.2018 **Väitöspäivä** 30.11.2018

Julkaisuluvan myöntämispäivä 12.10.2018 **Kieli** Englanti

☐ **Monografia** ☒ **Artikkeliväitöskirja** ☐ **Esseeväitöskirja**

Tiivistelmä

On tärkeää, että mittaustulokset eivät riipu paikasta tai ajasta. Tämä varmistetaan käyttämällä kansainvälistä mittayksikköjärjestelmää (SI), joka on toteuteuttu primääristen mittanormaalien avulla. Nämä normaalit ovat laitteita, joilla voi mitata tai tuottaa mittayksikköä vastaavan suureen arvon, ja joita ei tarvitse kalibroita toista saman yksikön toteutusta vastaan. Tässä väitöskirjassa tutkittiin mahdollisuutta luoda kvanttimittanormaalit kelvinille ja ampeerille. Lisäksi kehitettiin laitteita, jotka liittyvät tähän tutkimukseen tai ovat sen mahdollistajia.

Coulombin saartoon perustuvaa lämpömittaria tutkittiin mahdollisena primäärisenä mittanormaalina kelvinille: Sille rakennettiin mittausympäristö, jossa lämpötila voitiin määrittää Boltzmannin vakion ja jäljitettävästi mitatun jännitteen avulla. Lisäksi sitä verrattiin PLTS-2000 lämpötila-asteikkoon sekä kahteen muuhun Boltzmannin vakioon perustuvaan primääriseen lämpömittariin.

Ampeerin kvanttimittanormaalitutkimukseen sovellettiin kahta eri ilmiötä: elektronien tunneloitumista suprajohde - eriste - normaalimetalli (NIS) -liitoksissa ja kvanttivaihehyppyjä suprajohtavissa nanolangoissa. Väitöskirjan aikana jälkimmäisiä havaittiin uudessa materiaalissa, molybdeenisilisidissä. Teoreettisesti on todistettu, että suprajohteen korkea normaalitilan resistiivisyys on edullista kvanttivaihehyppyihin perustuvien normaalien toteutukselle. Tällainen resistiivisyys voidaan saavuttaa kyseisessä materiaalissa.

Virran kvanttimittanormaalin aikaansaamat signaalit ovat pieniä (suurimmillaan nanoampeereja) ja tästä syystä ylimääräinen kohina voi kasvattaa tarkkoihin mittauksiin tarvittavaa kestoa merkittävästi. Toisaalta taas, jos kohinafotonien energia on suuri, ne voivat rikkoa Cooperin pareja tai aiheuttaa epätoivottuja tunneloitumisia, mikä heikentää laitteiden tarkkuutta. Ensimmäinen näistä ongelmista ratkaistiin mittauskytkennän johdotusta parantamalla ja jälkimmäistä varten tutkittiin kahta kohinasuodatinta.

NIS-liitoksiin perustuvien laitteiden, mm. kvanttivirtanormaalien, tutkimuksessa saavutettua tietämystä hyödynnettiin kahdessa sovelluksessa: kohina-antureissa ja jäähdyttimissä. Jälkimmäisiä käytettiin jäähdyttämään millimetriskaalan piisiruja. Niissä jäähdytys perustui fononien liikkuvuuden rajoittamiseen toisin kuin aiemmin tutkituissa NIS-jäähdyttimissä. Samassa yhteydessä todettiin simulointeja apuna käyttäen, että jäähdytys 1,5 K:stä aina sataan millikelviniin asti on saavutettavissa oleva päämäärä.

Avainsanat kvanttifysiikka, mittatekniikka, tunneliliitokset, kvanttimittanormaalit, kelvin, ampeeri, jäähdytys, kohinasuodatus- ja detektointi, yksittäiset elektronit

ISBN (painettu) 978-952-60-8275-2 **ISBN (pdf)** 978-952-60-8276-9

ISSN (painettu) 1799-4934 **ISSN (pdf)** 1799-4942

Julkaisupaikka Helsinki **Painopaikka** Helsinki **Vuosi** 2018

Sivumäärä 153 **urn** http://urn.fi/URN:ISBN:978-952-60-8276-9

Preface

I started my graduate studies almost exactly five years ago in Centre for Metrology and Accreditation (MIKES). However, most of the work related to this thesis was carried out after MIKES merged to VTT Technical Research Centre of Finland Ltd at the beginning of the year 2015. Working at VTT has brought its benefits: It has provided synergies and collaborations that would have otherwise been hard to obtain, and for that I am grateful.

This thesis was supervised by professor Jukka Pekola from PICO group at Aalto University. I would like to thank him for believing in me, making this dissertation possible and supervising my thesis.

Even though my graduate studies started in late 2013, my journey into the world of metrology began already in summer 2010, when I came to MIKES as a summer student. From that summer onward Antti Kemppinen has been my mentor into the world of quantum current standards and low temperature measurements in general. That has been an interesting journey but not always an easy one. However, I appreciate that Antti has always found the time to be interested in my work. Without you the journey would have been much harder.

At the beginning there were just me and Antti Kemppinen, and sometimes Antti Manninen, doing the quantum current research. However, when time passed, Janne Lehtinen joined the group only to slip into more fabrication oriented work a few years later. Recently, I have also had the pleasure to partially supervise the master's thesis of Sahin Dursun and collaborate with Jaani Nissilä and Pekka Immonen.

In a metrology institute, quality is a key factor, and as a group leader Antti Manninen is the gatekeeper of quality in electricity. I do believe that all the hard question Antti has asked have made me a better researcher and my publications much better. On the other hand, Janne Lehtinen has always been easy person to talk to and he was also the one who introduced me to nanowires. Both excellent merits. From other quantum electronics people at MIKES, Jaani always has more ideas than time. Despite all that he did a fine job supervising one of my special assignments. Lately I've had the pleasure to work with Pekka and be subject to his quiet knowledge of low temperature measurements. However, despite all the excellent mentors, one can never truly master a subject before

she needs to explain it to others. This summer I was presented this opportunity as I watched Sahin Dursun's first steps into cryogenics. Sahin, it has been a pleasure to work with you.

During my years at MIKES and VTT, I have had the opportunity to collaborate with some brilliant minds. One of such person is Mika Prunnila, a master of semiconductor technology among other things, who has had the patience to guide me through some pitfalls when submitting to high-end journals. I was also fortunate to briefly work with professor-to-be Ville Maisi, as he co-instructed my master's thesis.

My PhD thesis would not have been possible without all of my co-authors. With some of you I have had the opportunity to collaborate closely and the rest of you I'd like to learn to know better. Thank you, Ossi Hahtela for introducing me to low temperature thermometry, Matthias Meschke for helping me during the early stages of my thesis and Dmitry Golubev for inventing theory for us. Thank you Leif Grönberg, Andrey Shchepetov, Andrey Timofeev and David Gunnarsson for your sample fabrication expertise and that I could analyze your brilliant cooler samples. Some of my research would not have been possible without the low-noise expertise of Dietmar Drung and his graduate student Christian Krause. I'd also like to thank all the rest of you: Leif Roschier, Jari Penttilä, Jost Engert, Alexander Kirste, Aya Shibahara, Andrew Casey, Lev V. Levitin, John Saunders and Sergey V. Lotkhov.

At the beginning of my thesis, I spent plenty of time in cleanroom and got familiar with people from PICO and QCD groups as well as some cleanroom staff. I'd like to than all of you for all the supplies I was able to borrow and all the help I've got in cleanroom, bonding, Python, soldering, asking autographs from von Klitzing and research in general. Oh, and of course for all the nights spent in bars after Physics days. Special thanks to Elsa Mannila, who made me some samples.

Even though I have spent plenty of time in cleanroom my desk has always been located at Tekniikantie 1. There I have had the pleasure to meet some brilliant metrologists and sometimes hear interesting stories about e.g. house renovating projects and history of MIKES, including how it acquired it hydrogen masers. I've also got plenty of help with e.g. PADS, Comsol and other software as well as finding noise sources in my setup. My work would have been much harder without the two workshop at Tekniikantie 1: the mechanical one and the one related to electricity, and great thanks goes to their maintainers.

Getting funding for basic research is not always quaranteed in Finland, and therefore I'd like to thank Wihuri foundation, Academy of Finland (project QuMOS), and European metrology programmes EMPIR and EMRP which are funded by EU and participating countries (projects e-SI-Amp, MICROPHOTON and Qu-Ampere), for enabling my work, and Martti Heinonen for taking the leap of fate and offering me permanent employment.

As fulfilling as it is to do research, there is still life outside the lab. My graduate life would have been much more empty without all the stories, mangas, books,

poetry nights, DnD sessions, console (and computer) game sessions, musical and anime watchings, sitsit, wappus, assemblys, new year parties, sauna nights, triple birthdays and all the other get-arounds just to name a few. I would like to thank all of you who have made these events possible, but especially Onerva, Milja H., Olli, Matti, Eetu, Aino, Anssi, Suvi and Antti. I'd also like to thank my dear parents Pentti and Sirpa, who have been a great support for me during my life. Its good to know that there is always a number to call if I don't know something and almost always a room for an overnight quest at their cottage.

Last but not least, I'd like to thank my beloved husband Jani Saarenpää. Thank you for supporting me during my graduate years and all the others before that (over ten years and counting!). Thank you for always listening, sharing a similar view of the world and often understanding what my work is about. Thank you for just being there.

Espoo, October 24, 2018,

Emma Mykkänen

Contents

List of Publications

This thesis consists of an overview and of the following publications which are referred to in the text by their Roman numerals.

I E. Mykkänen, J. S. Lehtinen, A. Kemppinen, C. Krause, D. Drung, J. Nissilä and A. J. Manninen. Reducing current noise in cryogenic experiments by vacuum-insulated cables. *Rev. Sci. Instrum.*, **87**, 105111 (7 pages) , 2016.

II O. Hahtela, E. Mykkänen, A. Kemppinen, M. Meschke, M. Prunnila, D. Gunnarsson, L. Roschier, J. Penttilä and J. Pekola. Traceable Coulomb blockade thermometry. *Metrologia*, **54**, 69 (8 pages) , 2017.

III J. Engert, A. Kirste, A. Shibahara, A. Casey, L. V. Levitin, J. Saunders, O. Hahtela, A. Kemppinen, E. Mykkänen, M. Prunnila, D. Gunnarsson, L. Roschier, M. Meschke and J. P. Pekola. New Evaluation of T - T-2000 from 0.02K to 1K by Independent Thermodynamic Methods. *Int. J. Thermophys.*, **37**, 125 (11 pages) , 2016.

IV J. S. Lehtinen, E. Mykkänen, A. Kemppinen, S. V. Lotkhov, D. Golubev and A. J. Manninen. Characterizing superconducting filters using residual microwave background. *Supercond. Sci. Technol.*, **30**, 055006 (10 pages) , 2017.

V E. Mykkänen, J. S. Lehtinen, A. Shchepetov, A. Timofeev, L. Grönberg, A. Kemppinen, A. J. Manninen and M. Prunnila. Efficient thermionic refrigeration and phonon isolation by a semiconductor-superconductor junction. Submitted , 2018.

VI J. S. Lehtinen, A. Kemppinen, E. Mykkänen, M. Prunnila and A. J. Manninen. Superconducting MoSi nanowires. *Supercond. Sci. Technol.*, **31** 015002 (7 pages), 2018.

Author's Contribution

Publication I: "Reducing current noise in cryogenic experiments by vacuum-insulated cables"

The author did most of the measurements, performed the data analysis and wrote the manuscript.

Publication II: "Traceable Coulomb blockade thermometry"

The author participated in the measurements and data analysis.

Publication III: "New Evaluation of T - T-2000 from 0.02K to 1K by Independent Thermodynamic Methods"

The author participated in the measurements.

Publication IV: "Characterizing superconducting filters using residual microwave background"

The author performed the simulations and data analysis together with the first author.

Publication V: "Efficient thermionic refrigeration and phonon isolation by a semiconductor-superconductor junction"

The author designed and performed the device characterization together with two co-authors. The author performed the data analysis and simulations. The author and sixth and eight co-author co-wrote the manuscript.

Publication VI: "Superconducting MoSi nanowires"

The author participated in the measurements.

1. Introduction

This thesis was inspired by two concepts: metrology and tunnel junctions. Metrology is the science of measurement and its application. It is needed to ensure that measurement results are reproducible at different instants of time and in different locations. The basis of metrology is the International System of Units (SI) maintained by the International Bureau of Weights and Measures (BIPM) and national metrology institutes (NMIs) [1]. The SI is utilized through measurement standards: stable devices that can controllably and reproducibly either produce or measure a value of quantity. If these standards do not need any calibration against any other standard for quantity of the same kind they are called primary standards and are a realization of the SI.

At the moment the SI is changing to a more fundamental direction: it will be defined by invariants of nature most probably in May 2019 [2, 3]. This thesis takes part on the research related to this change and explores two of the seven SI base units: the kelvin, which will be linked to the Boltzmann constant, k_B, and the ampere, which will be defined by the elementary charge, e. It also investigates devices that are byproducts of the research of these two or devices needed to enable them.

Tunnel junction and related theory are heavily utilized in this thesis. In Publication II we present a traceable measurement scheme and verification for Coulomb blockade thermometer (CBT) [4], a device which utilizes arrays of tunnel junctions between normal metal electrodes (NIN junctions), and where tunneling probability into a small volume between junctions is affected by the number of electrons in it. We also perform an intercomparison between CBT and two other thermometers (Publication III), an important method in metrology to verify the correct performance of devices.

The Coulomb blockade has a key role also on one of our two approaches to develop a standard for the ampere: Tunnel junctions between normal metal and superconductor (NIS junctions) are well understood and relatively simple in design [5]. They can be used to produce current, $I = ef$, related to elementary charge e and frequency f. They are, however, prone to tunneling of excess electrons or missed tunneling events and one cause of such events, quasiparticle formation in superconducting electrode, will be further discussed in this thesis

(unpublished data in section 4.2).

The physics behind NIS junctions is based on an approximation, the first order perturbation theory, and needs corrections to describe the error mechanisms. Devices that would be based on more fundamental physics, gauge invariance for example, would be more likely free of such errors, and superconducting nanowires are dreamed to be such devices. No consistent theory exists for them yet, but it has been proven that if tunneling of flux through them is coherent, they are an exact dual to Josephson junctions [6]. Josephson junctions are devices, where Cooper pairs tunnel through a weak link [7] and which are gauge invariant and experimentally verified to be independent of material parameters down to the relative uncertainty of 10^{-16} [8]. In Publication VI we do a research aiming at finding a perfect material for the future nanowire current standard.

Especially the NIS based current standards, but also other superconducting devices, suffer from high temperature and environmental noise. In addition, noise can also have a detrimental effect on low-uncertainty low-current measurements. These will be the topic of the remaining three publications of this thesis. Publication I is a study of cables aiming at decreasing measurement noise, and as such it is directly linked to improving the performance of all possible realizations of quantum current standard. Publication IV and Publication V utilize the NIS-junctions as noise sensors and coolers, respectively, and are byproducts of the study aiming at creating a NIS-based standard for the ampere. Publication IV provides, on the other hand, also supporting equipment for this standard since it studied the performance of two different noise filters.

In this thesis, we are mostly interested in temperature range from 20 mK up to about 3 K. We used aluminium as the superconductor in all the NIS-devices of this thesis, as it can produce stable native oxide and is commonly used to make tunnel junctions. It has a critical temperature of about 1.2 K (or higher in thin films), which sets the upper limit for the operations range of these devices. The research related to nanowires was extended up to little higher temperatures of about 3 K. The lower limit of our measurements is about 20 mK, which is set by the base temperature of the ^{3}He/^{4}He dilution refrigerator used to cool down the samples of this thesis. This temperature is sufficient for our purposes.

There are several ways to realize a thermometer in 20 mK - 3 K range. The SI defines the temperature through the international temperature scale ITS-90 [9] and its provisional low temperature extension PLTS-2000 [10]. From these the former is determined through melting and triple points of materials and it extends from 1357.77 K down to 0.65 K. The latter is based on properties of helium and ranges from 1 K to 0.9 mK. These scales are somewhat cumbersome, and especially the latter is difficult to realize in practice. However, for example different thermometers based on e.g. noise current in resistors [11, 12] operate in our temperature regime. Also CBT can be used in this temperature range as it has operation regime spanning from 4 mK [13] to 60 K [14].

All the present attempts to link the ampere to elementary charge need low temperatures [15]. They utilize quantum physics to generate current $I = ef$,

where frequency f can be extremely precisely determined with atomic clocks. Since the ampere is the base electric unit in the SI, all other electric units should link to it. However, its present definition is hard to realize experimentally [16] and in practice, the electric metrology is based on quantum standards of the volt and the ohm. They utilize Josepson effect [6, 17] and quantum Hall effect [18] and produce values of the quantities comparable to $K_{J-90} \simeq h/2e$ and $R_{K-90} \simeq h/e^2$, respectively. Here h is Planck's constant. In addition of being easier to realize than the present definition of the ampere, they are also internally very consistent. The best intercomparison results between two Josephson elements have relative uncertainties of about 10^{-19} [19] and consistency of quantum Hall standards has been tested down to relative uncertainty of 10^{-10} [20, 21]. The full potential of this consistency has yet to be utilized, however, since the correctness of these effects related to the present SI has not been verified below relative uncertainty of about 10^{-8}. A realization of a quantum current standard would thus have a two-fold purpose: It would, of course, be the direct realization of the future SI and could be used to calibrate devices with currents in the range of 10 fA...1 nA. In addition, it could be used, through Ohm's law, to verify the correctness of Josephson and quantum Hall effects. Though, to do this, currents of at least hundreds of picoamperes and relative uncertainty below 10^{-8} are needed [22], and these have not yet been simultaneously realized [15]. The best results so far have been obtained with semiconductor quantum dots [23, 24] and have reached relative uncertainties of about 0.16 parts per million (ppm) for current of about 100 pA and 20 ppm for 1 nA, respectively.

The refrigeration to the sub-K temperatures needs cryoliquid based equipment, which are large and expensive. These problems could be overcome with electronic coolers, but no practical device yet exists for our temperature range. Low temperature electric refrigeration has been studied in various quantum devices, for example, quantum dots [25], single ions [26], microelectromechanical systems [27], piezoresistive elements [28], cold atoms [29] or Coulomb blockade devices [30]. Here, however, we use aluminium based NIS-junctions, which have optimal operation around 300 mK and have been successfully used to cool mm- to cm-scale objects [31, 32, 33] from around 300 mK to 250–200 mK. The NIS junctions cool the normal part of the device, which is traditionally connected to a membrane cooling platform with cold fingers. The payload on the platform is refrigerated by phonon interaction. These devices work against the electron-phonon coupling in the cold finger, which is exponentially suppressed at low temperatures. This hinders the cooling at low temperatures due to too weak contact to the refrigerated object and at high temperatures because of too good contact to the substrate phonons. In Publication V we present a NIS-based cooler, which operates directly against the phonon interface conductance of the junction and that of the aluminium leads. We also study by simulations the effect of cascading junctions and ways to further hinder the heat leaks from the environment.

Especially the NIS-junctions [34], but also other superconducting devices [35,

36, 37], are sensitive to electromagnetic environment. At one point, the environmental noise was the limiting factor of NIS based quantum current standards [38] but filtering the noise and shielding the sample from it has improved the situation [38, 39, 35, 40]. Two on-chip filters are also studied in Publication IV. On the other hand, the noise sensitivity of NIS junctions can be used to our advantage, since they can be used as noise sensors [39, 41, 42, 43]. This was utilized also in Publication IV.

This thesis is organized as follows: Section 2 gives an overview of the theoretical background of the tunnel junction devices, section 3 discusses experimental methods, noise filtering and sample fabrication, section 4 introduces the quantum metrological devices studied in this thesis and section 5 discusses two applications – noise detection and cooling – that are byproducts of the research of NIS-junctions.

2. Theoretical background

2.1 NIS and NIN tunnel junction devices

This section introduces theory for both NIS (normal metal – insulator – superconductor) and NIN (normal metal – insulator – normal metal) junctions. Even though they are different in some very fundamental ways, most of the tunneling theory for both can be derived starting from the same equations.

2.1.1 Tunneling rate and current

A tunnel junction consists of an insulating barrier between two metallic electrodes, as shown in figure 2.1. If the barrier is thin enough the wave functions

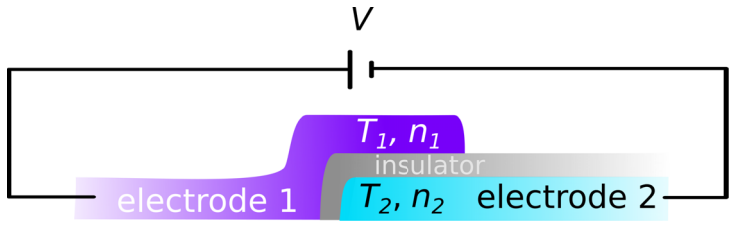

Figure 2.1. Schematic figure of what a tunnel junction can look like.

of electrons in the two electrodes can overlap and tunneling across the barrier is possible. The tunneling rate through such a junction, Γ, can be obtained from first order perturbation theory [44]. It depends on the junction transparency (or its tunneling resistance R_T), voltage V over it, and the properties of the electrodes. When an electron moves from the left lead to right ($-$) or vice versa ($+$) the tunneling rate is [44]

$$\Gamma(\pm eV) = \frac{1}{e^2 R_T} \int_{-\infty}^{\infty} dE n_1(E) f(E, T_1) n_2(\mp eV - E) f(\mp eV - E, T_2), \qquad (2.1)$$

where e is elementary charge, and T_i is the temperature and $n_i(E)$ is the relative density of states of electrode i. Here we have chosen the Fermi energy as zero

energy. The particles that tunnel through the junction are fermions and follow Fermi distribution

$$f(E,T) = \frac{1}{1+\exp(E/k_BT)}, \tag{2.2}$$

where k_B is Boltzmann constant. When tunneling from the left electrode to the right, term $n_1(E)f(E,T_1)$ tells the density of electrons on the left side of the junction and $n_2(-eV-E)f(-eV-E,T_2) = n_2(E+eV)[1-f(E+eV)]$ the density of vacant states on the right (and vice versa with reversed tunneling direction). Here we have assumed that the density of states is symmetric i.e. $n(E) = n(-E)$ and used the equality $f(E) = 1-f(-E)$, which holds for Fermi function. The current through the junction can be calculated as the difference between the tunneling to left and to right and is

$$I = e[\Gamma(eV) - \Gamma(-eV)]. \tag{2.3}$$

For NIN junctions both of the densities of states are usually approximatively constants i.e. $n_1(E) = n_2(E) = a$, where $a = 1$ with our normalization. Then, as long as $T_1 = T_2 = T$, equation (2.1) has a solution

$$\Gamma_{\mathrm{NIN}}(eV) = \frac{1}{e^2R_T}\frac{eV}{1-\exp(-eV/k_BT)}, \tag{2.4}$$

and the current becomes (see equation (2.3)) $I(V) = V/R_T$. This indicates constant resistance over the whole voltage span. However, experiments show that this is not always true, since e.g. finite barrier height [45] and dynamic Coulomb blockade [44] can alter the resistance. These can have detrimental effect especially to CBT, and special care needs to be taken in sample fabrication to minimize their effect.

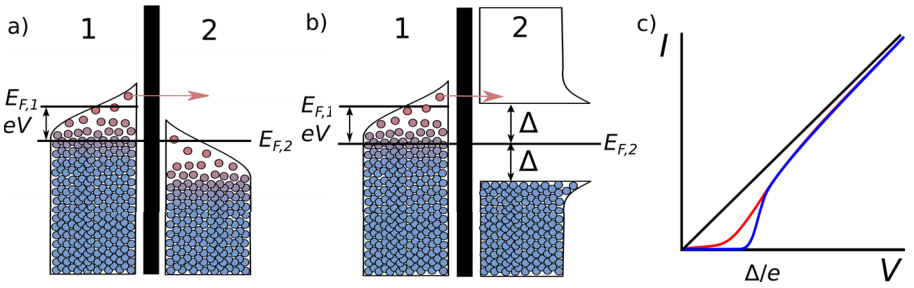

Figure 2.2. a) Energy diagrams for electrodes 1 and 2 in a NIN junctions. b) Energy diagrams for electrodes 1 and 2 in a NIS junctions. Electrode 1 consists of normal metal and electrode 2 of superconductor. The superconductor energy gap Δ blocks the electron transports to certain energy levels. c) IV-curves of NIS junction at two different temperatures (blue cold, red hotter) and the black line corresponding to $I = V/R_T$.

The densities of states are more complicated in case of NIS junctions. In superconductor most of the electrons are paired as bosonic Cooper pairs, which cannot live in the normal metal electrode. Forming a Cooper pair will bind energy and therefore breaking a pair will need it. In NIS junctions most of the current across the junction is thus carried by thermally exited electron-

or holelike quasiparticles. However, the Cooper pair binding energy, Δ, will create a band of forbidden energy levels around Fermi energy, which alters the relative density of states of these quasiparticles (see figure 2.2b). In case of ideal superconductor this density is [46]

$$n_S(E) = \mathrm{Re}\left(\frac{|E|}{\sqrt{E^2-\Delta^2}}\right). \tag{2.5}$$

Its effect on tunneling events is illustrated in figure 2.2b and on the current in figure 2.2c. From figures 2.2b-c and equations (2.1) and (2.5) one can see that when temperature is low, the tunneling rate and current are negligible in the energy gap (i.e. in region where $eV < \Delta$). This effect is, however, smeared and will be eventually destroyed when temperature rises and more and more electrons have enough energy to overcome the energy gap.

In most of the publications of this dissertation we did observe some leakage current in energy gap even at low temperatures, and equation (2.5) was not sufficient to describe the current characteristics. Therefore more complex model by Dynes [47, 48] was used:

$$n_{\mathrm{Dynes}}(E) = \left|\mathrm{Re}\left(\frac{E/\Delta + i\gamma}{\sqrt{(E/\Delta + i\gamma)^2 - 1}}\right)\right|. \tag{2.6}$$

Here γ is a Dynes leakage parameter, which can be determined as the ratio between the asymptotical resistance and the resistance in the energy gap at zero temperature, $\gamma = R_T/R_{\mathrm{gap}}$. The model (2.6) was first developed to describe the unidealities of the superconductor but later it was noticed that similar leakage can also originate from photon assisted tunneling [38].

2.1.2 Coulomb blockade and master equation

In the previous section we neglected the energy associated with electron tunneling through the junction. This energy is related to the energy needed to charge a capacitor with a single electron, the so-called charging energy, $E_c = e^2/2C$, and can become significant when temperature, T, and capacitance, C, are low, i.e. $k_B T \leq E_c$. If, in addition, the volume of at least one of the electrodes connected to the junction is small and the electrode is isolated, this energy can cause a situation, where tunneling of an electron into this isolated island can make further tunneling events energetically unfavorable [49, 50, 51]. This effect is called Coulomb blockade and it was present in all other publications and data, where NIS and NIN junctions are utilized, except for Publication V.

In this section we will study the situation of figure 2.3, where the isolated island is formed by connecting two tunnel junctions close to each other. The charge state of the island affects the overall electron transport and therefore the model of figure 2.3 contains also a gate electrode, which is capacitively coupled to the island and is used to contol its potential. This type of structure is referred as single-electron transistor (SET). The theory presented in this section is applicable to any of the combination of SINIS, NISIN and NININ, where the

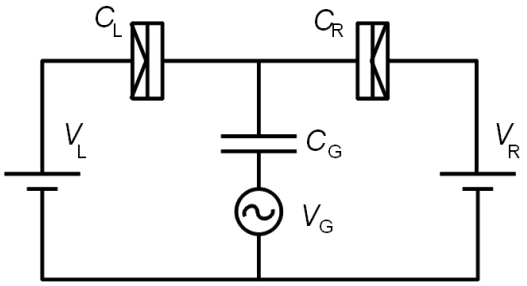

Figure 2.3. A network model of a structure with two tunnel junctions and a gate electrode [52].

innermost N or S represents the super- or normal conductivity of the island and outer N or S that of the electrodes.

The base energy of the island in the absence of bias voltage is

$$E_{\mathrm{ch}}(n) = E_c(n - n_g)^2, \tag{2.7}$$

where n is the number of excess electons in the island and $n_g = V_g C_g/e$ is the gate charge caused by the gate voltage, V_g, and capacitance between the gate electrode and the island, C_g. The characteristic energy needed to charge the island with a single electron, the charging energy, $E_c = e^2/2C_\Sigma$, is dependent on the sum of all capacitances in close vicinity of the island, i.e. $C_\Sigma = C_g + C_R + C_L + C_0$, where C_0 is the self capacitance of the island, and C_L and C_R are the capacitances of left and right junction respectively.

When an electron tunnels into (+) or out from (−) the island through junction i, the potential of the island changes from $E_{\mathrm{ch}}(n)$ to $E_{\mathrm{ch}}(n \pm 1)$ and energy $\delta E^{\pm} = E_{\mathrm{ch}}(n) - E_{\mathrm{ch}}(n \pm 1)$ is transported. When voltage V_i is applied over junction i we get the net change of island energy

$$\delta E_i^{\pm} = \pm 2E_c(n - n_g \pm 1/2) \pm e(V_i - \nu), \tag{2.8}$$

where the term ν comes from the unequalities of capacitances and voltages over the two junctions and is $\nu = (C_L V_L + C_R V_R)/C_\Sigma$, where V_L and V_R are the voltages of the left and right junction, respectively.

In section 2.1.1 the current could be obtained from equation (2.3). However, when consideration of multiple different charge states is needed things are more complicated. In finite temperatures the probability of a charge state n, $P(n,t)$, can be obtained using orthodox theory [15, 44]. In orthodox theory electrons tunnel one by one. With this assumption we obtain master equation

$$\frac{dP(n,t)}{dt} = -\Gamma_{n,n} P(n,t) + \Gamma_{n+1,n} P(n+1,t) + \Gamma_{n-1,n} P(n-1,t), \tag{2.9}$$

where

$$\Gamma_{n,n} = \Gamma_{n,n-1} + \Gamma_{n,n+1} \tag{2.10}$$

presents the transition rate out of state n and

$$\Gamma_{n,n+1} = \Gamma(\delta E_L^+(n)) + \Gamma(\delta E_R^+(n)) \tag{2.11}$$

$$\Gamma_{n,n-1} = \Gamma(\delta E_L^-(n)) + \Gamma(\delta E_R^-(n)) \tag{2.12}$$

the transition rates from state n to $n+1$ or $n-1$. Here the tunneling rate is obtained from equation (2.1). With these assumptions, the current becomes:

$$I = e\sum_n \left[\Gamma(\delta E_i^+(n)) - \Gamma(\delta E_i^-(n))\right] P(n,t) \tag{2.13}$$

The currents of NIN and NIS junctions are presented in figure 2.4. Two distinctive border conditions arise from the discussion of this section: When $n_g = 1/2$, we obtain the red curve of figure 2.4. This situation is referred as gate open, since the potential of the island is between two charge states and the tunneling energy is at its minimum. On the other hand, the situation with $n_g = 0$ is referred as gate closed and has the largest voltage region where current is small. All other IV-curves fall between these two curves.

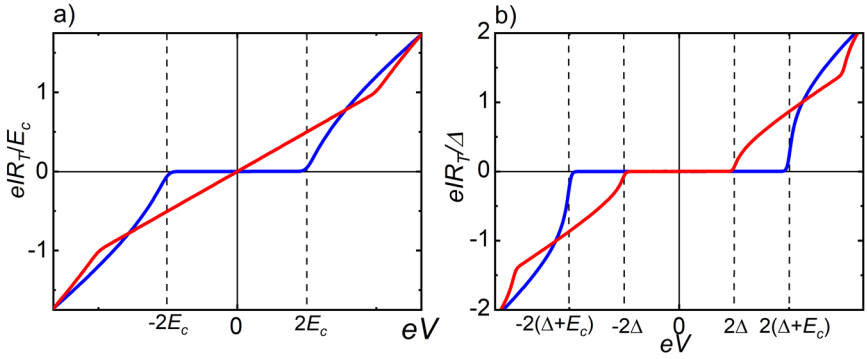

Figure 2.4. The IV-curves for NIN (a) and NIS (b) junctions in presence of Coulomb blockage. The figures are calculated for $E_c = \Delta$ and $\gamma = 10^{-6}$. The red curve presents the case $n_g = 1/2$ and blue curve the case $n_g = 0$. All other IV:s fall between these two curves.

2.1.3 Contact to environment and heat flow

From equation (2.1) we see that the temperature of the electrodes on each side of a tunnel junction will affect the charge transport across it. This is intuitive since the higher the temperature the more thermally activated tunneling events can happen. In this section we study the heat transport between the electrodes and their surroundings in order to obtain the temperatures of the electrodes.

The configurations of the samples of Publication II, Publication III, Publication IV and data discussed in section 4.2 were quite similar in the context of heat transport. In each, there were normal metal islands between tunnel junctions and all the structures were located on a silicon substrate. The heat configurations was, however, more complicated in Publication V, where the island was suspended by the junctions. In this section we will mostly discuss the heat

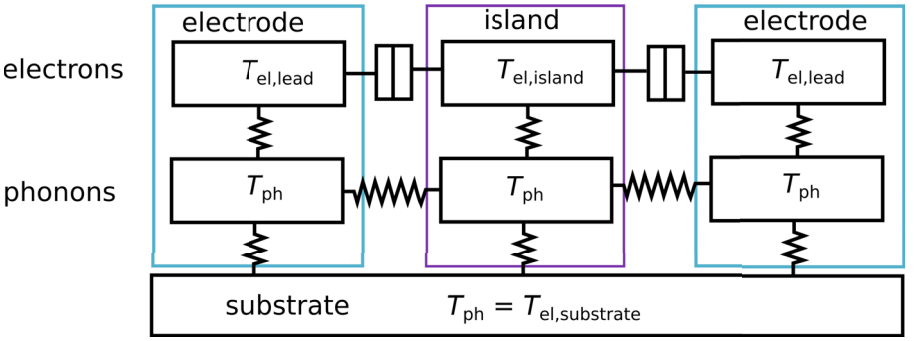

Figure 2.5. Thermal network of the samples in Publication IV, Publication II, Publication III and data of section 4.2 showing separate heat transport channels for electrons and phonons.

transport of Publication II, Publication III, Publication IV and data of section 4.2. Publication V will be discussed from those parts which coincide with the other publications and more thorough investigation is left to section 5.2.

The schematics of a heat transport network is presented in figure 2.5. In low temperatures and small structures, electrons and phonons need to be treated separately. This is also the case in the normal metal island. The phonon coupling between the substrate and the island is usually good and thus the phonons on the island are at the same temperature as those on the substrate. On the other hand, the electric heat conduction between the substrate and the island is weak due to the insulating nature of the substrate, and the main relaxation channel is the electron-phonon coupling in the island. This coupling is described by electron-phonon heat current

$$\dot{Q}_{e-p} = \Sigma\Omega(T_{\mathrm{ph}}^5 - T_{\mathrm{el,island}}^5), \tag{2.14}$$

which is valid for normal metals and where Σ is electron-phonon coupling constant (which is usually around 2×10^9 $\mathrm{Wm^{-3}K^{-5}}$ in copper [53]), Ω is the coupling volume and T_{ph} and $T_{\mathrm{el,island}}$ are the phonon and electron temperatures of the island, respectively. [53]

On the other hand, the heat flow carried by the electrons through a junction is [54]

$$q(\delta E_i^{\pm}) = \frac{1}{e^2 R_T}\int_{-\infty}^{\infty} dE(\delta E_i^{\pm} - E)n_{\mathrm{lead}}(E)f(E,T_{\mathrm{el,lead}})f(\delta E_i^{\pm} - E, T_{\mathrm{el,island}}), \tag{2.15}$$

where n_{lead} and T_{lead} are the density of states and temperature of the lead, respectively. The term $\delta E_i^{\pm}$ is the same as in equation (2.8) and simplifies to $\pm eV$, when both sides of the junction are infinite or the capacitance is large. The total heat flow into the island can be modelled similarly as equation (2.13) and is

$$\dot{Q} = \sum_{i=R,L}\sum_n \left[q\left(\delta E_i^+(n)\right) + q\left(\delta E_i^-(n)\right)\right]P(n,t), \tag{2.16}$$

where $\delta E_i^{\pm}$ is the net energy change when electron tunnels into the island (see equation (2.8)) and $P(n,t)$ is obtained from master equation (2.9). When the

charging energy is negligible equation (2.16) reduces to

$$\dot{Q} = \sum_{i=R,L} [q(eV_i) + q(-eV_i)]. \tag{2.17}$$

In steady state the heat flow into the normal metal and out of it must be equal and the electron temperature of the island can be solved from equations (2.14) and (2.16) or (2.17). If no external voltage is applied, the electrons and phonons are expected to be at the same temperature. Both equations (2.16) and (2.17) apply also to Publication V, but heat between island and the substrate is not mediated by electron-phonon coupling, since the island and substrate are not directly connected to each other.

When the leads are made of superconductors, electron tunneling creates a quasiparticle (hole or electron) in the leads, which degrades the performance of the device. This effect is strongest when a large number of quasiparticles pack near a tunnel junction. The quasiparticles relax through electron-phonon coupling and are transported away from the junction by diffusion. However, superconductivity suppresses the coupling and transportation can be significantly hindered if the superconducting lines are narrow.

Knowles et al. [55] studied this kind of effect when electrons were pumped through a SINIS turnstile with constant frequency f, and they noticed a high correlation between sample geometry and degradation of the performance. They modeled their findings with elevated superconductor temperature. We noticed, however, that such a simple model does not always completely describe this effect. Our findings will be further discussed in section 4.2.

The heat flow in the superconducting leads is also addressed in Publication V. There the main interest was the phonon heat conduction in the leads, which was observed to increase with increasing temperature above 500 mK in aluminium. This was most probably caused by increased electron-phonon coupling, which allowed electronic contribution in the heat transport. In Publication V the electron-phonon coupling in the superconductor, $\dot{Q}_{e-p,s}$, was modeled according to Ref. [56], where $\dot{Q}_{e-p,s} \approx \Sigma\Omega T_{\mathrm{el,lead}}^5 \exp(-\Delta/k_B T_{\mathrm{el,lead}})$ and which is strictly valid only when the phonon temperature in the lead is much smaller than the electron temperature and both of these are well below critical temperature of the superconductor.

2.2 Brief introduction to Josephson junctions and phase slips

The full theory of superconductivity is beyond the scope of this thesis. However, this section will discuss those parts that are needed in order to understand the results of Publication IV and Publication VI.

2.2.1 Josephson junctions

A Josephson junction is a structure, where two superconductors are connected by a weak link. Such a weak link can be, for example, a constriction in a superconducting wire or a thin layer of insulator. The Josephson junctions follow the so called dc and ac Josephson equations [46],

$$I_J = I_c \sin\phi \tag{2.18}$$

and

$$\dot{\phi} = \frac{2e}{\hbar} V, \tag{2.19}$$

respectively, where I_c is the critical current above which superconductivity vanishes, V is the voltage over the junction and e and $\hbar$ are the elementary charge and Planck constant respectively. The term $\phi = \chi_1 - \chi_2$ describes the difference of phases of the macroscopic wavefunctions, $\Psi(x) = |\Psi(x)|e^{i\chi(x)}$, of the two superconducting electrodes in each side of the junction.

Equations (2.18) and (2.19) are usually not enough when modelling real systems, since the junctions contain some amount of capacitance and current carried by quasiparticles. When the Josephson junctions are large, the system can be treated semi-classically and the so-called resistively and capacitively shunted junction model (RCSJ) can be used. This model is depicted in figure 2.6a and, as its name indicates, contains capacitance, C, and resistance, R, in parallel to the junctions. The total current through such a device is

$$I = I_c \sin\phi + \frac{V}{R} + C\frac{dV}{dt}. \tag{2.20}$$

When equations (2.19) and (2.20) are combined we get a second order differential equation

$$I = I_c \sin\phi + \frac{\hbar}{2eR}\dot{\phi} + C\frac{\hbar}{2e}\ddot{\phi} \tag{2.21}$$

which adequately describes the time evolution of the system.

This equation, in general, has no analytic solution, but can be understood quantitatively by studying the energy associated with it. In these calculations we will ignore the resistance, R, since it corresponds to the normal current carried by quasiparticles and its contribution is small well below the critical temperature of the superconductor, T_c. The energy associated with the system can thus be obtained as a time integral of equation (2.21) multiplied by V, which leads to

$$-\frac{\hbar}{2e}(I\phi + I_c\cos\phi) = +\frac{1}{2}C\left(\frac{\hbar}{2e}\right)^2\dot{\phi}^2. \tag{2.22}$$

Equation (2.22) has an analogy in mechanics and can be interpreted as a particle at position ϕ with kinetic energy $E_{\text{kin}} = \frac{1}{2}C\left(\frac{\hbar}{2e}\right)^2\dot{\phi}^2$ moving in the "washboard" potential

$$U_{\text{pot}}(\phi) = -\frac{\hbar}{2e}(I\phi + I_c\cos\phi) = -E_J\left(\frac{I}{I_c}\phi + \cos\phi\right), \tag{2.23}$$

where $E_J = \frac{\hbar}{2e}I_c$ is the Josephson coupling energy. The washboard potential is presented in figure 2.6b.

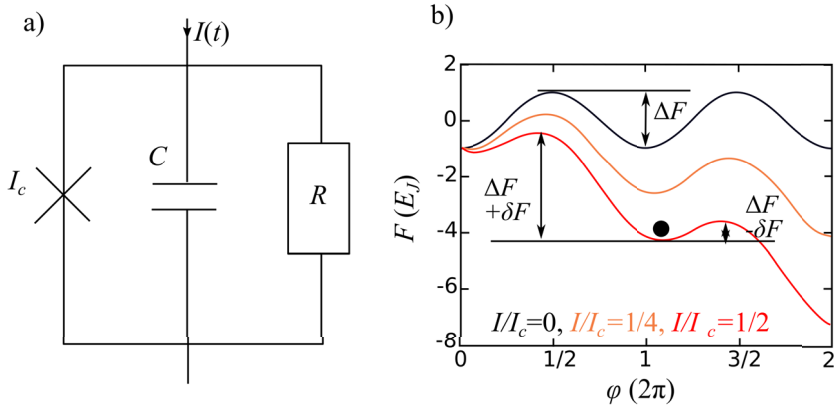

Figure 2.6. a) The electric network for the RCSJ model. b) Washboard potential depicting effects in Josephson junctions in context of RCSJ model

2.2.2 Superconducting quantum interference devices

Superconducting quantum interference devices (SQUIDs, see figure 2.7) are used in Publication IV as tunable filter elements. They consist of two Josephson junctions in a loop. The current through a SQUID is a sum of the currents of the individual Josephson elements, i.e. $I_{\mathrm{SQ}} = I_{c1}\sin(\phi_1) + I_{c2}\sin(\phi_2)$, where I_{ci} and ϕ_i are the critical currents and phase differences of element i.

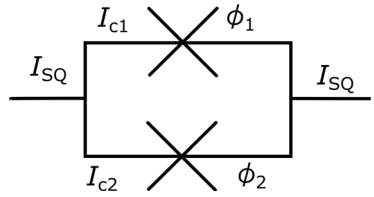

Figure 2.7. Superconducting quantum interference device

When the loop is exposed to a magnetic flux Φ, an additional current will be introduced in it. On the other hand, when a current is circulating in a wire, it will create a magnetic field. Here we will assume that the latter effect is negligible. Then the external flux creates a difference between ϕ_1 and ϕ_2, which follows $\phi_1 - \phi_2 = 2\pi\frac{\Phi}{\Phi_0}(\mathrm{mod}2\pi)$, where $\Phi_0 = h/2e$ is the magnetic flux quantum [46]. Combining this with I_{SQ} and using simple trigonometric tricks gives the critical current of the SQUID, $I_{\mathrm{SQ,c}} = \sqrt{I_{\mathrm{c1}}^2 + I_{\mathrm{c2}}^2 + 2I_{\mathrm{c1}}I_{\mathrm{c2}}\cos(2\pi\Phi/\Phi_0)}$. In Publication IV we assumed that the two Josephson elements are approximately equal. Then the critical current simplifies to $I_{\mathrm{SQ,c}} = 2I_{\mathrm{c1}}|\cos(\pi\Phi/\Phi_0)|$.

2.2.3 Phase slips

Phase slips are events, where the phase of the superconducting order parameter abruptly changes by 2π. According to ac Josephson equation (2.19), a change of

phase will induce a momentary voltage difference across superconductor, even though the system would otherwise be current driven and dissipationless. This can be interpreted as a magnetic vortex tunneling through the superconductor, and it induces momentary and localized suppression of superconductivity. In 2D and 3D structures this has no observable consequence, since a single resistive spot is not large enough to block the conduction of supercurrent through the whole structure. On the other hand, the situation is different in 1D structures, which is illustrated in figure 2.8.

The coherence length, ξ, defines the dimensionality of a superconductor since it describes the distance over which $\Phi(x)$ can vary without undue energy change, or in the concept of weak-coupling BCS theory, the size of a Cooper pair and thus the minimum size of a superconducting element or a normal metal section inside a superconducting element. A superconductor is n-dimensional if at least n of its dimensions are larger than the coherence length. This means that if a resistive region appears in a 1D structure, it will always be larger than two of the dimensions of the structure and thus block the transport of supercurrent as shown in 2.8.

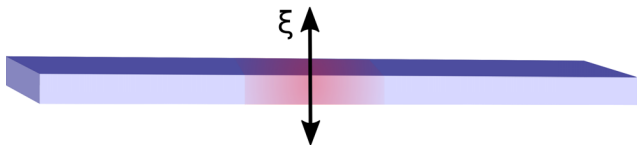

Figure 2.8. . The size of a normal metal element inside a superconductor is proportional to coherence length. When the coherence length is larger than two of the dimensions of the superconducting structure, the structure is considered one dimensional and a normal metal section can form that completely suppresses superconductivity for a limited range of the structure.

Phase slips can be quantitatively understood in the context of "wasboard potential" introduced in figure 2.6b. In this concept the phase is localized in a local minimum of the potential and it can either jump over the surrounding "hills" or tunnel through them. The jumps can occur as thermally activated processes (TAPS), where the surrounding environment gives the energy needed for the process. From figure 2.6 we see that this energy is $\Delta F = 2E_J$, when no current is present, and will change as $\delta F = E_J \frac{I}{I_c} = \hbar I/2e$, when current is applied. We know that tunneling rate is proportional to $e^{-\Delta F/k_B T}$, and thus the rate to the preferred direction is

$$\frac{d\phi}{dt} = \frac{2eV}{\hbar} = \Omega\left[\exp\left(\frac{-\Delta F_{\text{right}}}{k_B T}\right) - \exp\left(\frac{-\Delta F_{\text{left}}}{k_B T}\right)\right], \tag{2.24}$$

where $\Delta F_{\text{left}} = \Delta F + \delta F$ and $\Delta F_{\text{right}} = \Delta F - \delta F$ are the heights of the potentials in each side of the phase, and Ω is attemp frequency [57]. Now

$$V = \frac{\hbar\Omega}{e}\exp\left(\frac{-\Delta F}{k_B T}\right)\sinh\left(\frac{\delta F}{k_B T}\right) = \frac{\hbar\Omega}{e}\exp\left(\frac{-\Delta F}{k_B T}\right)\sinh\left(\frac{\hbar I}{2ek_B T}\right). \tag{2.25}$$

When I is small enough the hyperbolic sine can be approximated by its argument

and we get

$$R_{\mathrm{TAPS}} = \frac{V}{I} = \frac{\pi\hbar^2\Omega}{2e^2 k_B T}\exp\left(-\frac{\Delta F}{k_B T}\right). \tag{2.26}$$

The term ΔF is in theory just $2E_J = \hbar I_c/2e$, but in practice more elaborate models are needed to describe it. Since equation (2.26) depends exponentially on $-1/T$, the thermally activated phase slip events die out when temperature is decreased. However, experiments show residual resistance even at low temperatures [58, 59, 60, 61, 62, 63]. This can be explained by tunneling of phase.

These tunneling events are called quantum phase slips (QPS) and they need a microscopic theory to be fully understood. However, approximations can be made using a similar model as above as long as $\Delta F/k_B T$ is replaced with $S_{\mathrm{QPS}} = \Delta F/E_{\mathrm{ch,qps}}$. Here $E_{\mathrm{ch,qps}}$ is the characteristic energy scale of a QPS process in analogy to thermal processes where the characteristic energy scale is given by $k_B T$. Then the voltage associated with the phase slips is

$$V_{\mathrm{QPS}} = \frac{\hbar\Omega}{e}\exp\left(-S_{\mathrm{QPS}}\right)\sinh\left(\frac{\hbar I}{2eE_{\mathrm{ch,qps}}}\right). \tag{2.27}$$

As above, when I is small, equation (2.27) simplifies to

$$R_{\mathrm{QPS}} = \frac{V_{\mathrm{QPS}}}{I} = \frac{\Omega\pi\hbar^2}{2e^2 E_{\mathrm{ch,qps}}}\exp(-S_{\mathrm{QPS}}), \tag{2.28}$$

which can be written as

$$R_{QPS} = \frac{R_q\hbar\Omega}{\Delta}\exp(-S_{\mathrm{QPS}}), \tag{2.29}$$

when we assume that $E_{\mathrm{ch,qps}} = \Delta$. Here $R_q = h/(2e)^2$ is the resistance quantum. Equation (2.29) can explain the QPS events relatively well when $T_c/2 < T < T_c$, but use of microscopic theory is needed in lower temperatures. In Publication VI we studied the phase slip events in molybdenium silicide. Equation (2.26) was used to describe the thermal behavior of the results of Publication VI, and the microscopic counterpart of (2.29) [64, 65] was used to describe the tunneling events.

3. Experimental methods

This section summarises the measurement and sample fabrication techniques crucial or specific for this work.

3.1 Cryogenic methods

We used a cryostat which utilized pulse tube cooled dilution refrigerator [66] capable of achieving 20 mK temperature. The wiring and shielding inside the cryostat needed to be designed with care: If thermalizations are not done properly a sample does not cool down. On the other hand, electromagnetic noise can deteriorate the performance of the sample and hinder the measurements.

In this thesis, the noise is divided into two categories depending on whether it can cause quantum effects. In tunnel barrier devices the tunneling threshold energy sets the limit between these two: if the noise photons have higher energy than this, they can initiate unwanted tunneling processes. In NIS junctions this energy is comparable to the superconducting energy gap, which corresponds to temperature $\Delta/k_B \approx 2.5$ K or frequency $\Delta/h \approx 50$ GHz in aluminium, which is commonly used as the superconductor in NIS junctions due to its stable native oxides. Below we will speak about low frequency and high frequency noise, since the frequency of the noise is usually easy to extract.

As discussed above, the high frequency noise can cause unwanted tunneling events. It can also break Cooper pairs into quasiparticles. On the other hand, the low frequency noise causes spreading of the bias voltage, which smears the features of the output signal of the device under study. The low frequency noise also increases averaging times needed in measurements, which can change the duration of an experiment from hours to weeks making the measurements unpractical. In our experiments, the biasing side tolerated usually more noise than the measurement side. This is especially true in quantum current source experiments, where very low currents need to be measured with very high accuracy.

We used two kinds of measurement lines which were labeled as rf and dc lines. The rf lines were designed to work from 1 MHz upwards and the dc lines from

dc up to few hundred hertz. All the signals that were measured were carried by the dc lines. In our setup, the thermalization of dc lines was done by connecting long enough portion of them to the respective temperature flange. Similar kind of methods can also be used to thermalize the rf lines. However, the electrical losses in them are the higher the longer the line and this should be taken into account in the design. To further hinder unwanted heat leaks of rf lines we used dc blocks as heat blocks. They prevent the flow of direct current and low frequencies but let rf signals through without interference. The thermalization of the center conductor of rf lines was enhanced by using attenuators to connect the conductor to the outer shield and thus create a thermal contact.

3.1.1 Minimizing the effect of low frequency noise

The low frequency noise can be suppressed with classical room temperature filters. In case of rf lines also dc blocks can be used. In addition, the dc lines have usually some amount of capacitance and if they are also resistive, they act as RC filters further decreasing the low frequency noise. Thus the coupling of the noise to the bias signal was not a problem in our experiments. However, the situation was different when measuring currents produced by a quantum current standard, since very low uncertainties were needed.

In Publication I we investigated different cables and cable assemblies in order to reduce the low frequency current noise. In our setup, majority of the noise originated from the mechanical vibrations caused by the pulse tube precooler, which coupled to the measurement cables through tribo- and piezoelectric effects. The former effect arises from friction between insulator and conductor of the cable and the latter is due to mechanical stress of the insulator. The two can be hard to distinguish but triboelectric effect is assumed to have higher contribution [67]. Since the pulse tube refrigerators are popular, similar noise problems arise also in many other laboratories.

In our experiments, we were mostly interested in milliherz regime (long averaging times) and few hertz regime. In some other experiments, for example those related to quantum information, also higher frequencies may be of interest and studies of the kHz range has been made elsewhere [67].

In Publication I almost all studied cables were coaxial. It is known from room temperature experiments that polyethylene (PE) has usually lower noise compared to PTFE (teflon). However, we noticed that in the milliherz range properly minimizing friction may be more crucial than the material of the insulator, since the PTFE cable with graphite coating performed better than a pure PE insulated cable. This difference vanished when the measurement time was decreased. In addition, the best performance was obtained in cable assembly, where PE insulated room temperature cable, self-made vacuum insulated cable and PTFE+graphite insulated low temperature cable were combined. This is intuitive, since the PTFE+graphite cable was demonstrated to perform adequately, PE is generally a low-noise insulator and no tribo- or piezoelectric effects can

manifest in vacuum. In conclusion, we managed to push the cable noise down to the same range as that created by the amplifier.

Special care is needed when choosing a current amplifier for quantum current standard (and other low uncertainty) measurements. We used model DDPCA-300 from Femto and ULCA that was developed by Physikalisch-Technische Bundesanstalt (PTB) [68, 69, 70]. Femto DDPCA-300 had lower inherent noise but it can exhibit drifts in time. In the measurements aiming at the validation of a quantum current standards, it can be used as a null instrument, but its gain is too unstable for direct current measurements. Better choice for these measurements would then be ULCA, a device which is designed for this purpose. The ULCA inhibits higher noise than the Femto model DDPCA-300, but it is stable in time and temperature and can be calibrated directly against quantum resistance standard making it easily traceable.

3.1.2 Minimizing the effect of high frequency noise

The high frequency noise can penetrate down to the sample as electromagnetic radiation through vacuum (or air) or through cabling. In our experiments, the former route was suppressed by using two rf tight shields [39, 35], and the latter by using commercial attenuators and filters in rf lines, and self-made powder filters [71] in dc lines. Utilizing resistive coaxial cables as dc lines has also been shown to diminish the noise [72] and such cables were used as filters at the 20 mK stage in some of the measurements.

In addition to these off-chip methods, also on-chip filters can be used. These include e.g. resistive environments [40], SQUID filters [73, 74] and capacitive shunts [38], latter of which was also utilized in section 4.2. The filters can have different performance depending on the frequency range and noise level. In Publication IV we studied two tunable on-chip filters, a SQUID filter and a modified version of the capacitive filter, in a low noise environment in frequency range from 50 GHz to 200 GHz. The environment was achieved by using the off-chip filtering and shielding discussed in previous paragraph. The frequencies correspond to the range, which can be detected with aluminium-based NIS detector (see section 5.1 for detail) and which is thus detrimental for aluminium-based SINIS quantum current standard.

The capacitive shunt filter consisted of an aluminium ground plane and titanium electrodes. Its filtering properties improved near the critical temperature, T_c, of our titanium films, which was around 110 mK. The low T_c of our samples most likely originates from impurities that were formed due to strong gettering behaviour of titanium and residual gases in the evaporator. The improvement of filtering properties was unexpected since in the frequency range we are interested in, $f > \Delta_{\mathrm{Al}}/h$, the photons have at least five times more energy than is needed to break Cooper pairs in the titanium lines. In this limit titanium should be resistive regardless of temperature. However, the behavior of our filter was at least semi quantitatively explained by assuming that the titanium elec-

trodes consisted of weakly connected grains, which had a significant capacitance between them.

The frequency range posed also some amount of trouble for the other filter studied in Publication IV: SQUIDs are devices, where two Josephson junctions are connected in a loop and they are usually hard to model above $f \approx 20 - 200$ GHz. However, in Publication IV a reasonably good agreement with measurement results could still be achieved by using a standard superconducting theory. The SQUIDs can be considered as Josephson elements with magnetic flux (Φ) dependent inductance $L_J = \Phi_0/(2\pi I_c(\Phi))$ and critical current $I_c(\Phi)$ (see section 2.2.2). In Publication IV we modeled them as a transmission line with inductance L_J and some amount of self capacitance and resistance. These components then created an LCR-filter, which could be controlled by external magnetic field.

In conclusion, Publication IV demonstrated that our two filters can bring predictable and tunable additional filtering in the residual low-noise regime, which is present after the off-chip filtering and shielding.

3.2 Virtual lock-in amplifier

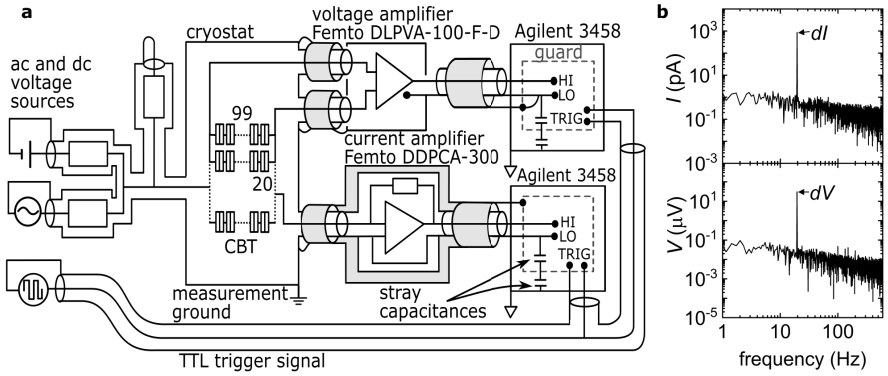

Figure 3.1. a) Virtual lock-in measurement setup used in Publication II and Publication III. b) Fourier transform of the measured voltage and current signals.

Instead of traditional lock-in amplifiers we used a sampling technique utilizing our accurate multimeters and post-processing Fourier transforms. This technique provided traceability and decreased noise, which was especially important in Publication II but was also useful in Publication III, Publication V and Publication VI.

The measurement setup of Publication II and Publication III is introduced in Figure 3.1. A modified version of this setup was used in the other two publications. Figure 3.1 shows that different channels of the digital-to-analog converter (DAC) voltage source were used to produce ac and dc biases and that they were adjusted with resistive voltage dividers to utilize the full output voltage range of the DAC. The DAC could be operated with floating ground and

this allowed us to specify a single grounding point, other than the DAC, for the electric network. In our case the body of the cryostat was chosen as this point.

In the measurement side, we used current and voltage amplifiers from Femto and a multimeter Agilent 3458, which is the equipment-of-choice of metrologists throughout the world and is known for its high accuracy and properly done groundings and guards.

The cables between the sample and the multimeters were triaxial. In the current measurement, the outer shield of the cable was connected to the cryostat ground and to the so-called guard shield of the multimeter. In voltage measurement, the outer shield was used to provide the ground to the multimeter, since the voltage amplifier was isolated. The purpose of the triaxial cables in current measurements was to guide noise currents in the outermost conductor, which does not carry the small measurement signal. Such noise currents can be introduced e. g. by magnetic field that couples in ground loops that are closed by stray capacitances.

A sinusoidal wave was used to bias the sample and a square wave TTL signal to sync the multimeters as shown in figure 3.1a. We used Agilent 34951A module as the DAC, which has 200 kHz point-to-point update rate and 16 bits of resolution. We measured a sequence with an integer number of cycles of the sine,N_c, which is necessary for both obtaining the dc bias over the sample and properly extracting the amplitude of the measured signal. The first is simply the average voltage during the sequence. As an example of the latter, in the measurements of Publication II and Publication III we used a sine drive with frequency of about f_{SIN}=19.53 Hz (10240 points with 200 kHz point-to-point update rate of DAC) and triggering signal with frequency of f_{TRIG}= 1176.47 Hz (170 points). These frequencies produce measured data with exactly N_c=68 cycles when Agilent 3458A digitizes N=4096 voltage samples. Then $N_c/f_{\mathrm{SIN}} = N/f_{\mathrm{TRIG}}$. Finally, the amplitude of the measured signal was obtained by Fourier transforming the signal and recording the height of the peak at drive frequency (see Figure 3.1b).

In the measurement setup of Publication V only ac voltage was recorded. In addition, since additional bias voltages were connected to the device under test (DUT) we wanted to galvanically isolate the virtual lock-in. This was done by utilizing optoisolators and using capacitively coupled alternating current bias. In Publication VI we used alternating current bias and voltage measurements.

3.3 Sample fabrication, i.e., overview of nanofabrication methods

All the publications of this thesis had distinguished samples whose fabrication schemes deviated from each other (a brief overview of these methods is listed in table 3.1). Therefore, this sections gives a brief introduction to the relevant methods rather than explains each publication separately. It is divided into four parts, describing different processing steps: patterning, material deposition or removal, oxidation and annealing.

Table 3.1. Overview of fabrication methods used in the publications of this thesis

Publication II Publication III	1. aluminium sputtering 2. patterning and etching 3. native oxide removal → in-situ oxidation inside sputter → aluminium sputtering 4. patterining and etching
Publication IV	1. aluminium ground plane deposition 2. growing SiO_2 with PECVD and titanium dc-line deposition 3. three-angle evaporation and in-situ oxidation using aluminium and gold palladium 4. lift-off
Publication V	multiple processing steps involving: etching, sputtering and in-situ oxidation of silicon inside sputter. The tunnel junctions are formed between doped silicon wafer and aluminium leads
Publication VI	1. patterning on pure silicon wafer 2. patterning, native oxide removal and molybdenium sputtering 3. lift-off 4. annealing to form molybdenium silicide
unpublished data on SINIS	1. gold ground plane deposition 2. oxide deposition and patterning 3. angle evaporation and in situ-oxidation using aluminium and copper 4. lift-off

The patterning was done with either optical or electron beam lithography utilizing both negative and positive resists. In both lithography methods the polymers in the resist are strengthened (negative resist) or weakened (positive resist) when exposed to radiation (i.e. either light or electrons). After the exposure, the weak bonds are removed by a dedicated liquid. In this work, optical lithography was done by using separate masks (usually colored glass or plastic) between the light source and the resist. In contrary, no masks were needed in electron beam lithography, where the patterning was done by moving the electron beam. This makes the latter method more versatile but also slow, especially when writing bigger structures. On the other hand, it has a higher resolution compared to optical lithography and is therefore used to make nanoscale samples.

The pattern is transferred from the resist to the final material either with etching or by a lift-off method. Etching can be used to pattern metals, semiconductors etc. but also native oxide of wafers. It is performed either by different

liquids or by gas bombardment and removes material at the areas exposed in the lithography step. Different etchers affect different materials and in specific cases stop layers can be used to protect other layers of the sample from the etcher. In this thesis, outside of the native oxides of Si and Al, the materials to be etched were deposited by sputtering or electron beam evaporation.

When using etching, the material is deposited before etching step or resist spinning. In lift-off processes the situation is reversed: the material is deposited only after the resist is patterned and developed, and the structures are formed where there are holes in the resist. A specific subgategory of the lift-off method is the angle deposition, where a cave is formed inside the resist and the metal deposition is done in different angles (see figure 3.2). This method can be used to make in-situ tunnel junctions with suitable oxidation scheme and without exposing the deposited materials to ambient air.

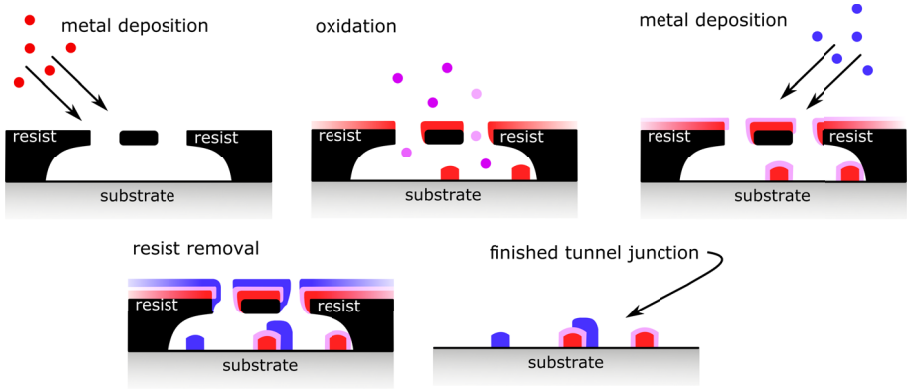

Figure 3.2. Fabrication steps in two angle evaporation.

In this thesis oxides were used for two different purposes: to form tunnel junctions and to insulate layers of conducting materials. All the tunnel junctions were formed with in-situ techniques, where the oxidation is directly followed by material deposition and the sample is not exposed to ambient air in between. Outside of the angle-evaporation scheme, also combination of sputtering and etching can be used to form in-situ tunnel junctions. However, then the bottom electrode needs to be fabricated in separate processing step and its native oxide removed before the oxide deposition, for example by argon milling. In both of the in-situ methods described above a controlled amount of oxygen is brought inside the vacuum can of the evaporator or sputter and it is allowed to make a native compound with the exposed material. After the oxidation another layer of material is deposited on top of the newly formed oxide. The in-situ methods were used to form tunnel junctions. When stronger, more insulating oxide was needed, we used ex-situ methods, e.g. plasma enhanced chemical vapour deposition (PECVD) or atomic layer deposition (ALD).

Publication VI used also annealing, where the sample is heated to high temperatures. In this case the annealing allowed deposited molybdenium to form a compound with the silicon wafer.

4. Quantum metrology

4.1 Quantum Phase Slips

4.1.1 Quantum current standard with superconducting nanowires

It has been shown theoretically that when the QPS events are coherent, the QPS is an exact dual to large Josephson junctions [7]. This means that the theories of these two are mathematically equivalent under the change of variables of phase and charge. Since coherent QPS (CQPS) has been proven to exist [75], this opens up a unique yet largely unexplored opportunity for metrology: Large Josephson junctions, which follow the RCSJ model (see section 2.2.1), have been used as quantum voltage standards since 1960s as they can produce quantized voltage steps, called Shapiro steps [17]. If a dual of these devices could be fabricated, it would then produce similarly quantized current steps. In addition, CQPS could also be used to replace Josephson junctions in many applications. For example, charge [76, 77] and flux [78] detectors have already been demonstrated.

Current standards based on CQPS would have important advantages compared to single-electron devices. In QPS the effects can be made coherent in contrast to the SET devices. They would also be based on more fundamental physics and could thus become equally accurate as Josephson voltage standards.

However, so far no consistent measurement results exist that would have demonstrated current steps with reasonable accuracy, though some attempts and results have been acquired [79]. It is believed that the normal state resistivity of the nanowires should be high in order for the steps to be visible. The importance and the effect of resistive environment is still not yet clear. For example, the steps might be smeared due to the coupling of electromagnetic environment to the nanowire [80] or heating in the resistive environment [81]. It has also been shown that large disorder of chemical potential can induce a so-called Bose glass transition, which would prevent the observation of quantized current steps [82].

It should also be noted that the nanowires are not the only devices that could

be dual to the large Josepson junctions, as also a chain of small Josephson junction can be used for this purpose. However, there the background charge fluctuations seem to lead to an inevitable Bose glass transition [82].

4.1.2 Initial phase slip results in molybdenium silicide

In this thesis, we focused on preliminary material study. We demonstrated QPS in novel material: molybdenium silicide (MoSi). This is shown in figures 4.1a-b: Typical features of QPS are e.g. the resistive tail at low temperatures and negative magnetoresistance. Both of these are observed at the narrowest nanowire whereas a slightly wider wire behaves as a normal superconductor when temperature is decreased. The figure 4.1a also contains QPS and TAPS fits introduced in section 2.2.3.

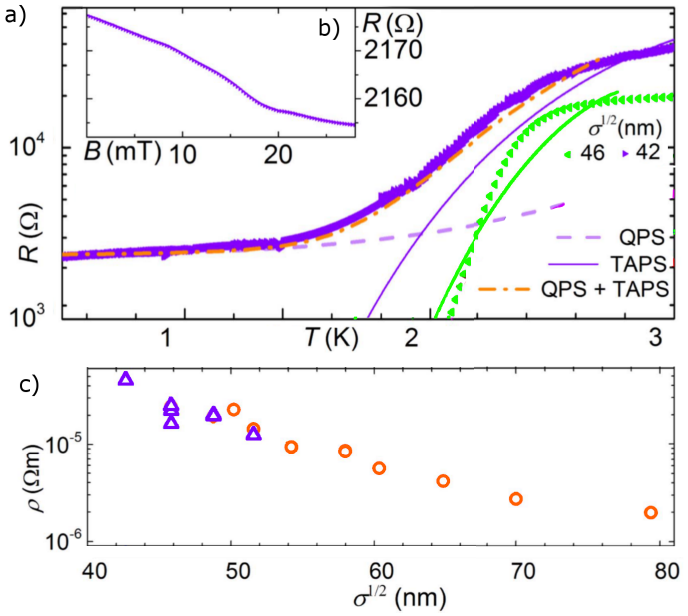

Figure 4.1. a-b) The resistance of a nanowire with 42 nm effective diameter (purple dots) as a function of temperature (a) and magnetic field (b), and the resistance of slightly larger nanowire (46 nm, green) as a function of temperature (a). c) Low temperature normal state resistivity of nanowires as a function of the effective diameter. Different colors represent different number of thermal treatments: samples that were annealed only once are marked as orange and samples that were re-annealed after initial treatment are marked as purple. The annealing had no significant effect on the data. This is also evident in (a), where the wire with diameter 46 nm has data from measurements after both anneals. The smaller wire was measured only after latter anneal. All the measurements were performed in 4-probe geometry and the lines had length of 2 μm.

Our sample layout, which was used for these first material tests, could not be used to indicate coherence. However, we observed that the low temperature normal state resistivity of the nanowire, measured at about 4 K, could be tuned both by changing the effective diameter of the wire (see figure 4.1c) as well

as changing the annealing time or temperature. In addition, some samples had higher normal state resistivities than shown in figure 4.1c but issues with contact quality between bonding wires and the samples prevented measuring them at low temperatures. Another interesting observation was that even though the first annealing had a high impact on sample characteristics, the samples seemed to be impervious to further changes if annealed a second time. Since high normal state resistivity is expected to be essential for observing the current steps, these makes MoSi and other superconducting silicides made with similar process promising materials.

4.2 SINIS turnstile as quantum current standard

The beginning of experimental work on this thesis was dedicated to investigation of the SINIS turnstile as a potential quantum current standard. SINIS is a promising device, with solid theoretical background, easily parallellizable design and a theoretical ultimate relative accuracy of about 10^{-8} [5]. It also provides a platform for studying interesting physical phenomena. During this thesis an attempt to parallelize the turnstiles was performed, but the parallelization ultimately failed due to sample fabrication problems. In addition, we performed a study of non-thermal quasiparticles in SINIS turnstile, which gave new interesting data, but the results were not published because no model to explain the findings was found. Some of the results of these studies are summarized here.

4.2.1 Theory of charge pumping and parallelization

Pumping electrons

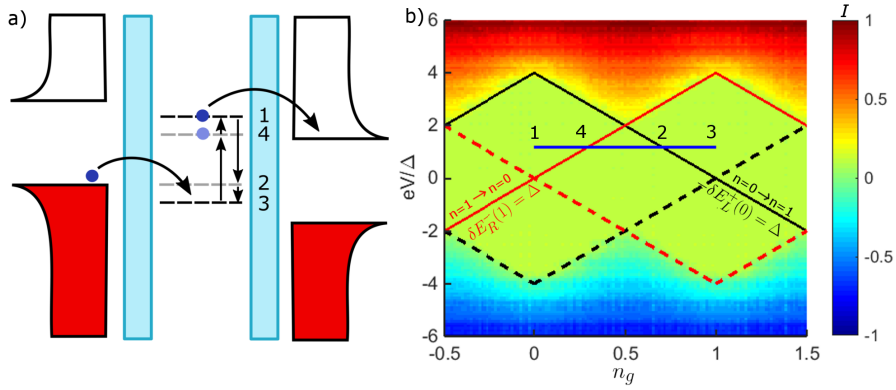

Figure 4.2. a) A schematic representation of electron states in the normal metal and superconductor. b) The effect of gate charge and bias voltage on the current through the SINIS turnstile

When a SINIS turnstile is used as a quantum current source it is operated

with constant bias voltage and alternating gate voltage. At low temperatures equations (2.1) and (2.8) give the tunneling thresholds into (+) or out from (-) the island through junction i

$$-\delta E_i^{\pm}(n) = \mp 2E_c(n - n_g \pm 1/2) \mp eV_i \geq \Delta. \tag{4.1}$$

When these thresholds are crossed charge transport becomes probable. The charge pumping process is illustrated in figure 4.2. The black and red solid and dashed lines in figure 4.2b represent the tunneling thresholds.

The charge transport proceeds as follows. We first start at point 1, where the most likely charge state is $n = 0$ and no excess electrons are present in the island. Then the potential of the island is decreased (n_g is increased). When point 2 is crossed, tunneling into the island becomes probable. The probability of tunneling can be still slightly increased by further decreasing the potential, but one should note that unwanted tunnelings to the wrong direction (dashed line) or even tunneling of excess electrons (furthermost solid line) will be enabled if the potential is decreased too much. In addition, the bias voltage usually oscillates a little due to noise, and it is a good practice not to bring the potential too close to the undesired thresholds. Therefore we stop somewhere around point 3. Now an electron has entered the island from the left lead. To transport this electron into the right lead, the potential is increased (n_g is decreased) up until point 1. The tunneling out of the island into the right lead will become probable when point 4 is crossed but as before the probability can be increased by moving beyond this point and therefore we increase the potential up until point 1.

Main error sources

The processes that cause the largest errors for the operation of the SINIS turnstile are thermally activated tunneling, higher order tunneling processes, leakage in the energy gap and quasiparticle formation in the superconductor. Thermally activated tunneling arises from the finite temperature of the environment. This type of error mechanism can never be fully suppressed and it sets a limit for the relative accuracy of SINIS turnstile, which is about 10^{-8}, when the bias voltage is set to an optimal point ($eV_b = \Delta$) and temperature is below 100 mK [5].

On the other hand, even without the thermal activation, tunneling of wrong number of electrons is possible. From the most simple higher order processes elastic ones are negligible and simplest in-elastic process, co-tunneling, is energically forbidden in the BCS-energy gap [83]. Thus the only relevant higher order processes are Andreev reflection and Cooper pair/electron cotunneling (CPE). In Andreev reflection a Cooper pair tunnels through a junction, whereas in CPE a Cooper pair tunnels into the island simultaneously as a electron tunnels out of it (or wise versa). The Andreev reflection is suppressed when gate amplitude A_g is smaller than $A_{\mathrm{g,Ar}} = \frac{1}{2} - \frac{\Delta}{2E_c}(1 - \frac{eV_b}{2\Delta})$ [83], indicating that the higher the E_c the better. When E_c is increased above 2Δ, $A_{\mathrm{g,Ar}}$ will become larger than the

backwards tunneling threshold (dashed lines in 4.2) and further increase is no longer that beneficial.

On the other hand, the relative error created by CPE is the weaker the higher the pumping frequency f. However, when frequency is increased the chance that no electron is transported also increases. Ref. [83] studied this tradeoff theoretically and concluded that when $E_c = 2\Delta$ and as long as current stays below 10 pA ($f \approx 60$ MHz), relative error rate of 10^{-8} can be achieved.

The leakage in the superconducting energy gap is either due to photon assisted tunneling (PAT) [38] or quasiparticle states within the gap [84]. In the semiconductor-superconductor (Sm-S) tunnel junctions studied in Publication V it can also originate from traps and dopants in the junctions [85]. Saira et al. [34] have shown that in good NIS junctions this leakage mainly originates from PAT and corresponding Dynes leakage parameter (see equation (2.6)) can be pushed to $\gamma = 1.6 \times 10^{-7}$, which is sufficient for charge pumping. During this thesis, however, these levels were not reached due to sample fabrication problems. These problems most likely originated from the contamination of the evaporator resulting in unideal tunnel junctions and leakage in the energy gap of the order of 10^{-5} to 10^{-4}.

In the absence of the sample fabrication problems, the main error source which limits the accuracy of SINIS is the formation of quasiparticles. Some amount of quasiparticles are always present due to the thermal background but their number is small and their effect can usually be ignored. In SINIS turnstile, however, quasiparticles are also created when electrons are transported through the system. These quasiparticles can become a problem, if they can linger near the tunnel junctions, which is the case if the superconducting leads are long and narrow [55], and such structures should therefore be avoided.

Parallellization scheme for a sample where everything is taken into account
Figure 4.3 presents a parallelization scheme and a close up image of a SINIS device. The sample geometry is optimized for performance. The charging energy is inversely proportional to the junction size and thus small junctions are needed. On the contrary good quasiparticle relaxation needs superconducting leads that are large in all three dimensions and which widen fast [86]. This is enabled by three angle evaporation scheme, where first a thin layer of aluminium (c. 15 nm) is deposited to form the base of the tunnel junction and then the angle is changed to make another layer of aluminium. This layer is thick and is located as close to the tunnel junction as possible. When both aluminium layers are ready the sample is oxidized and then normal metal island is deposited. Due to background charges, each turnstile needs its own dc gate. These charges do not affect the ac gate, however, and thus all samples can be biased with the same ac drive. This is beneficial, since it decreases the complexity of the design. In addition, using separate ac cables would increase the thermal stress in the cryostat. The design also incorporates a ground plane, which is buried underneath the leads. This ground plane filters the high energy photons, suppressing electromagnetic

leakage (see section 3.1.2).

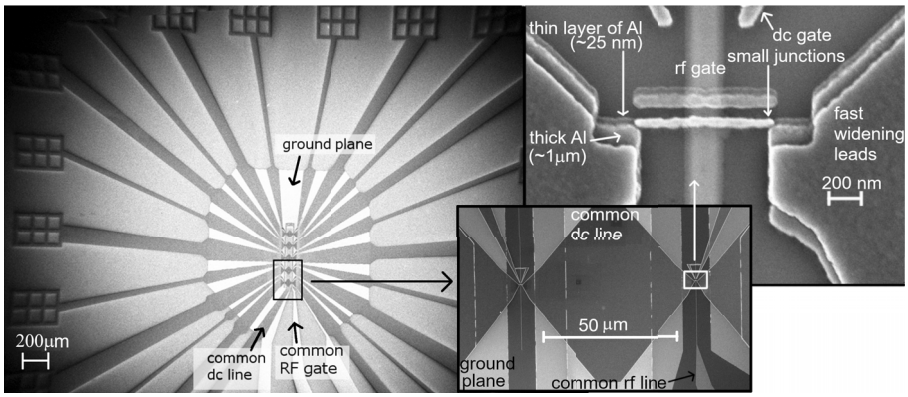

Figure 4.3. Scanning electron micrographs of SINIS devices connected in parallel on chip. The design features a common rf gate and a common drain lead for all junctions. All the leads are identical near the junctions. In this design we made junctions on both sides of the common drain lead to optimize the usage of space. Both sides are symmetric with each other. The junctions were made with three-angle evaporation scheme to enable thick layer of aluminium near tunnel junctions.

The sample design discussed above would incorporate all the necessary components for high accuracy charge pumping with increased current output. However, as discussed before, the samples studied during this thesis suffered from subgap leakage which degraded their accuracy. In addition, some problems were also encountered during EBL-patterning, since the size of the tunnel junctions was at the edge of the resolution of the electron beam writer and in addition the large aluminium leads caused some extra residual dose near them.

4.2.2 Non-thermal quasiparticles

As discussed above, currently the most significant error source of SINIS turnstile is quasiparticle formation (as long as fabrication anomalies are neglected). Here we will study this process in a sample that has been intentionally engineered to have a poor quasiparticle relaxation. This sample was made by two angle evaporation technique using 25 nm thick aluminium leads, native aluminium oxide barrier and 30 nm thick copper island. The sample geometry and measurement setup are presented in figure 4.4a and the relevant sample parameters obtained from current voltage characteristics (figure 4.4b) and SEM images in table 4.1. The sample is driven with sinusoidal gate voltage, which alters the gate charge as $n_g = \frac{1}{2} + A_g \sin(2\pi f t)$, where f is drive frequency. It should also be noted that Andreev reflections were present in our sample due to relatively small charging energy. However, this process caused only small effect in the current since the Andreev rate scales as $1/R_T^2$ (whereas the 1e-rate depends on $1/R_T$) and the junction resistance of our sample was large. The negligible effect of Andreev tunneling was also verified with simulations (data not shown).

The measurements were performed as null measurements, where the signal

Table 4.1. Sample parameters (see section 2.1.2 for detail). Here A_{ch} is the phenomenological area of a quantum channel related to Andreev tunneling, A is the area of tunnel junctions, and l is the length of the narrow portion of the line. *Since our tunnel junction transparencies are of the same order of magnitude as in Ref. [87], we have used similar A_{ch} as they.

E_c/Δ	Δ μeV	γ	R_T kΩ	A_{ch} nm^2	A nm^2	l μm	C_L/C_Σ %	C_R/C_Σ %	C_0/C_Σ %	C_g/C_Σ %
1.04	236	small	1359	30*	c. 3500	20	55	35	8	2

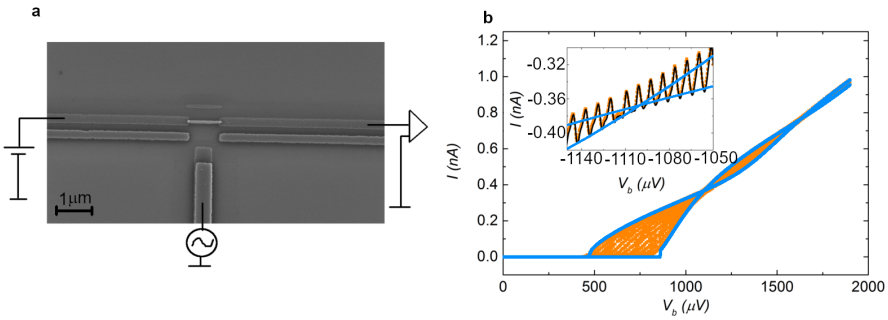

Figure 4.4. a) Measurement setup and sample geometry, b) IV-characteristic and related fits. The orange lines are obtained by simultaneously stepping bias and gate voltages and measuring current at each point. The oscillation comes from moving between gate open and gate closed states. The blue lines are simulations at gate open and gate closed positions. In the inset more elaborate simulation is given (black line). Here, instead of constant gate voltage, the voltage is allowed to vary according to the true signal. In ideal case all the orange and black lines should fall between the blue ones. This is not the case in our sample that has asymmetric junctions.

of the SINIS was compared to that produced by calibrated equipment (voltage source and resistor) [88]. The SINIS turnstiles can usually be modelled with high accuracy [52, 89], however, during this work we observed discrepancy with theory, which could yield new physics. The pumped current can be obtained from equation (2.13) by utilizing the knowledge of tunneling rates (2.1) and the time evolution of the probability distribution of charge state. The master equation (2.9) can be used to obtain the latter either by making consecutive small steps in time or incorporating time evolution in exponential matrixes as in [89]. The temperature of the island is obtained by iteratively finding a temperature that balances heat flows (see section 2.1.3).

Figure 4.5 presents pumping characteristics for our sample at five different frequencies (1 MHz, 3 MHz, 10 MHz, 20 MHz and 50 MHz) and four different bias voltages (160 μeV, 180 μeV, 220 μeV, 250 μeV). The figure can be interpreted as follows: *(i)* The measurement results deviate from the simulations: the simulations underestimate either the increase of current at A_g = 0.6 or the decrease of current at higher gate amplitudes. *(ii)* The discrepancy between simulations and measured data seems to grow when pumping frequency is increased. *(iii)* The green line in figure 4.5e, which is simulated with T_S = 50 mK and corresponds to bias voltage of 160 μeV, underestimates the current drop at

$A_g = 1.1$. This indicates that the current drop cannot be explained with simple thermal models. The situation is similar at 50 MHz.

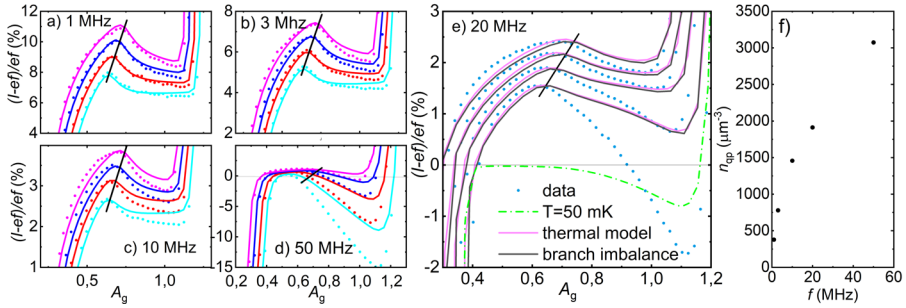

Figure 4.5. a)-d) The deviation of measured currents from $I_{\mathrm{ref}} = ef$ (produced by calibrated voltage source and resistor) when the SINIS device is operated as a turnstile (dots) for bias voltages V_b =160 μV (cyan), 180 μV (red), 220 μV (blue) and 250 μV (magenta) at frequencies 1 MHz (a), 3 MHz (b), 10 MHz (c), and 50 MHz (d), and corresponding simulations utilizing the theory of section 2.1 (solid lines of similar color). The solid black lines indicate the thresholds after which backwards tunneling starts. The quasiparticle temperatures of the simulations are a) 292 mK for all curves, b) 315 mK for all curves, c) 336 mK (cyan, red) and 337 mK (blue, magenta) and d) 360 mK for all curves. e) The deviation of measured current from ef when the SINIS device is operated as a turnstile (blue dots) at 20 MHz at the same bias voltages as in a)-d). The light magenta line corresponds to similar thermal model simulations as in a)-d) but at quasiparticle temperature of 349 mK, whereas the dark gray line shows data when different branches are at different temperature (80 mK for the cold branch, 370 mK for the hot one). These two models yield almost identical results. The green dashed line shows the current for bias voltage of 160 μV when superconductor temperature is set to 50 mK. f) Quasiparticle density as a function of pumping frequency.

The temperature of superconductor is related to quasiparticle density by a simple equation $n_{\mathrm{qp}} = 2D(E_F)\int_0^\infty dE n_S(E) e^{-E/k_BT} \approx \sqrt{2\pi} D(E_F)\Delta\sqrt{k_BT/\Delta} e^{-\Delta/k_BT}$, where $D(E_F)$ is the normal state density of states at the Fermi energy. Figure 4.5f shows the quasiparticle density, extracted from figures 4.5a-e, as a function of pumping frequency. Effect of geometry on the pumping frequency of SINIS has been studied before by Knowles et al. [55]. However, they found that n_{qp} depends linearly on frequency, which is not the case in figure 4.5f. Our measurements differs from their in that our quasiparticle densities in figure 4.5f are about ten times higher than theirs [55]. These results may indicate that at higher n_{qp} traditional models no longer apply. The differences in densities between data shown in this thesis and those of Ref. [55] are likely a result of different superconducting lead geometries and the higher normal state resistivity of our sample.

So far, we have used a constant value for the quasiparticle temperature. This is not strictly true, since the temperature depends on the power injected into the superconductor, which in turn depends on the current. However, the current changes only a few percent on the plateau, which is unlikely to cause great variation in temperature. This was verified with simulations utilizing similar heating power as in equation (2.16) and knowledge of the quasiparticle density extracted from geometry, see Ref. [55]. The simulations showed (data not shown)

that the temperature variations were no larger than a few millikelvin. Such variations caused only very small effect on the simulated curves.

The simulations described in previous paragraph were used to estimate the normal state resistivity of aluminium in our sample, which was 0.9 – 1.2 $\mu\Omega$m. This is about 30-40 times higher than the literature value for bulk Al at room temperature. However, the normal state resistivity of the thin electrodes depends on the sample fabrication process, e. g. on the resulting grain size and the amount of residual oxygen in the evaporators.

When electrons tunnel through a SINIS device they are extracted from the lower quasiparticle branch of one lead and injected to the upper branch of another. In theory, this can create imbalance between the branches in a lead. This effect was tested in figure 4.5e, where the quasipartcle-rich branches were set to 370 mK and the quasiparticle-void branches to 180 mK. Figure 4.5e shows that branch imbalance has negligible effect on the current of a SINIS device.

To lower the effect of quasiparticles, it is crucial to get them transported away from the tunnel junctions as fast as possible. In narrow lines, quasiparticle relaxation is small and this happens mainly via diffusion. On the other hand, the diffusion rate of quasiparticles depends on their energy, which is neglected in the models described above. In addition, in some situations the energy distribution of these particles may differ from Fermi function. However, we were unable to find any model that would have explained the results of figure 4.5 and thus they are not published elsewhere.

4.3 Primary thermometry

There are two types of standards: primary and secondary ones. Vast majority of the standards fall into the latter category. The properties of these standards can change over time and they need repeated calibration against other standards of the quantity of the same kind. The correct reading of the secondary standards is ensured by an unbroken chain of calibrations that can be traced back to the present definition of the SI, realized by the primary standards. In thermometry, a typical example of a secondary standard is a resistive thermometer. Its temperature behavior is dependent on geometry and material, and for example thermal or mechanical stress can change it.

The primary standards are based on well known physics. They can be divided into two categories: absolute and relative devices [90]. The absolute devices need no calibration against any other instance of the unit, though they might need calibration against other SI units. For relative thermometers, calibration needs to be done exactly once.

This thesis studies the utilization of a Coulomb blockade thermometer (CBT) [4] as a primary thermometer. The CBT consists of an array of NIN junctions connected in series, and it is based on the fact that its electric conductance changes as a function of temperature (see figure 4.6). It follows the theory introduced

in section 2.1 though with slight modification of the charging energy. When all of the junctions are identical and the biasing is symmetric, this energy becomes $E_c = \frac{N-1}{N}\frac{e^2}{C_\Sigma}$, where N is the number of junctions, $C_\Sigma = 2C + C_0$, C is the capacitance of a junction and C_0 is the self capacitance of an island [4].

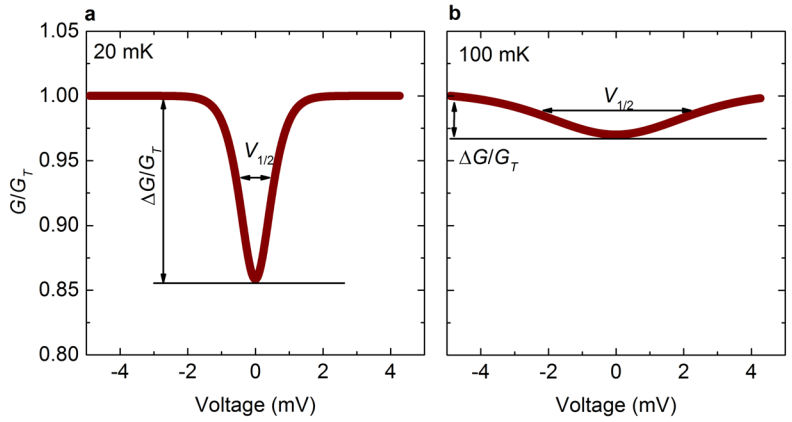

Figure 4.6. The normalized electric conductance of a CBT that is optimized to work at low temperatures.

In the weak Coulomb blockade regime ($E_c \ll k_B T$) the full width of the conductance dip of CBT at half minimum [4]

$$V_{1/2} \cong \frac{5.439 N k_B T}{e}, \tag{4.2}$$

depends only on constants and the CBT can be used as absolute primary thermometer. However, measuring the full conductance curve is slow. The temperature can also be obtained from the conductance dip at zero bias, ΔG,

$$\frac{\Delta G}{G_T} = \frac{1}{6} u_N, \tag{4.3}$$

where $u_N = E_C/k_B T$ and which is faster to measure. However, this method needs the knowledge of E_c and asymptotic conductance G_T. Neither of these constants depend on temperature and they can be determined at a single fixed temperature point using equation (4.3), which makes the conductance dip measurements relative primary thermometry.

In Publication II and Publication III we operated at temperatures between about 20 mK and 200 mK, which includes a shift from weak Coulomb blockade regime at 200 mK to intermediate Coulomb blockade regime ($E_c \sim k_B T$) at lower temperatures. In the latter, equations (4.2) and (4.3) need to be expanded to yield more accurate results

$$V_{1/2} \cong \left(1 + 0.3921 \frac{\Delta G}{G_T}\right) \frac{5.439 N k_B T}{e} \tag{4.4}$$

$$\frac{\Delta G}{G_T} = \frac{1}{6} u_N - \frac{1}{60} u_N^2 + \frac{1}{630} u_N^3. \tag{4.5}$$

The linear correction of (4.4) depends only on $\Delta G/G_T$ and does not change the primary nature of the equation. In Publication II and Publication III we used equation (4.5) as well as the full theory introduced in section 2.1 to explain our results.

In Publication II a virtual lock-in amplifier (see section 3.2) was used to provide a traceable measurement setup and improved accuracy to the CBT. The publication compared the results to superconducting fixed point thermometer (SRT), which was calibrated against PLTS-2000 and thus provided traceability to the present SI. In addition, in Publication III we performed an intercomparison between CBT and two other primary thermometers. This kind of intercomparison are crucial for metrology and provide verification for devices with different phenomenological background or different fabrication environment. All the results of Publication III yielded an agreement within better than 1 %.

It should also be noted that there exist only a couple of realizations of PLTS-2000 and these realizations start to deviate from each other below about 10 millikelvin [91]. An intercomparison of different primary thermometers below this temperature could thus provide improvements to accuracy of the present PLTS-2000. However, thermometry at these temperatures was not studied in this thesis.

5. Applications

5.1 SINIS as a spectrum analyzer

The presence of high energy electromagnetic environment (photons with frequencies f for which $hf \leq k_B T$, where h and k_B are Planck's and Boltzmann's constants and T is temperature) is detrimental to tunnel junction devices, since it can initiate unwanted tunneling events. On the other hand, this sensitivity can also be used to probe the environment [41, 42, 43, 39]. A NIS-type device was used for this purpose in Publication IV, which investigated two tunable on-chip filters in low noise environment, which was present after off-chip filter and shielding (see section 3.1.2). The measurements were performed at the frequency range detectable by (and thus detrimental to) aluminium based NIS junctions.

A NIS junction is a tunable integrating detector that can detect photons with higher frequency than that needed to initiate a tunneling process. Its threshold frequency can be altered by adjusting the electrostatic energy difference $\delta E_i^{\pm}$ introduced in equation (2.8). In Publication IV we used a detector scheme described in figure 5.1, which followed that introduced in Ref. [42]. It consisted of two parts: a monitoring island, whose charge state n could be controlled with voltages V_g and V_s, and a SINIS turnstile which was used to detect this charge state. When a photon ignited a tunneling event, it changed n, which in turn altered the gate charge of the detector SINIS and thus its voltage. In the measurements we used only small bias currents for the detector SINIS, since excess current creates random telegraph noise, which can produce significant errors when measuring small signal levels [34].

The detector scheme of figure 5.1 had two major limitations. The first is related to sample fabrication and is easy to fix in future iteration rounds: The middle island of the two leftmost tunnel junctions could not be controlled and therefore, even though δE could be fixed, its exact value was not known and it needed to be extracted from the fits. The latter limitation is, however, of a more fundamental origin: When a device utilizing charging effects is used as a detector, it cannot

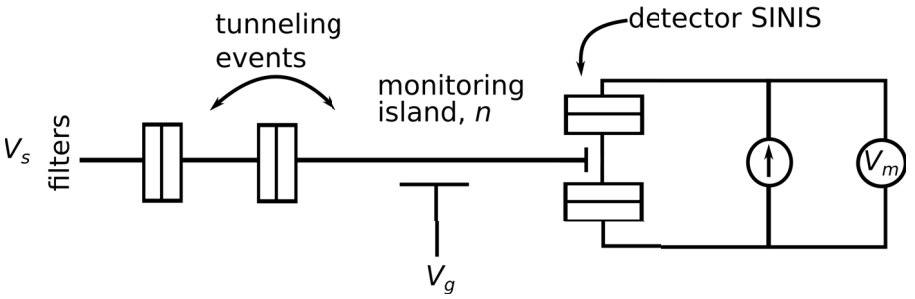

Figure 5.1. Noise detection scheme used in Publication IV.

be matched to either the common transmission line impedance of 50 Ω or to the vacuum impedance (377 Ω). This is due to the fact that the charging effects become notable only when impedance of the detector is larger than the quantum impedance $R_K = h/e^2 \approx 25.8$ kΩ. This means that only a fraction of incident photons can be detected. However, this kind of detector can still be used to deduce the relative performance of filters as was done in Publication IV.

The effect of the electromagnetic environment on a NIS junction can be modeled by adding a probability to absorb ($E < 0$) or emit ($E > 0$) photons, $P(E)$, to the tunneling rates [44]

$$\Gamma(\delta E_i^{\pm}) = \frac{1}{e^2 R_T} \int_{-\infty}^{\infty} dE n_S(E)[1 - f(E, T_S)] \int_{-\infty}^{\infty} dE' f(E - \delta E_i^{\pm}, T_N) P(E - E'). \tag{5.1}$$

Here indices N and S refer to normal metal and superconductor, respectively. The latter integral is a convolution of $f(E)$ and $P(E)$, which causes smearing of $f(E)$ as shown in figure 5.2. When $P(E) = \delta(E)$, i.e. the environment is an electromagnetic void, equation (5.1) simplifies to the familiar form of equation (2.1).

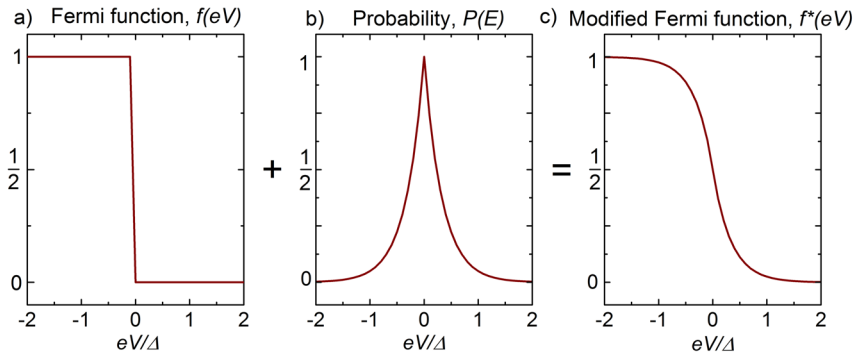

Figure 5.2. a) Fermi-function at zero temperature. b) Approximation $P(E) = \exp(-a|x|)$ c) Convolution of a) and b) showing that the sharp steplike behaviour of a) gets smeared when noise is introduced.

In theory, $P(E)$ could be solved from equation (5.1) simply by using Fourier transforms, since the Fourier transform of a convolution is a product, and

equation (5.1) consists of two convolutions. In reality, however, the practical implementation of this is hard, since the standard Fourier algorithms expect the functions to approach zero relatively fast, whereas the value of Fermi functions $f(E)$ approaches zero at ∞ but remain finite at $-\infty$. In Publication IV, we used an indirect method: standard theory for $P(E)$ was used in combination with the knowledge of the used filter, as described below. This led to a model with only few variable parameters, which could be extracted by comparing the tunneling rates of equation (5.1) to the measured ones.

As long as the first order perturbation theory and equation (5.1) hold, the energy exchange probability is [44]

$$P(E) = \frac{1}{2\pi\hbar}\int_{-\infty}^{\infty} dt\ \exp\left[J(t) + \frac{i}{\hbar}Et\right]. \tag{5.2}$$

In addition, in the presence of electric network environment with complex impedance $Z_t(w)$ we get the phase-phase correlation function

$$J(t) = 2\int_{-\infty}^{\infty}\frac{d\omega}{\omega}\frac{\mathrm{Re}[Z_t(\omega)]}{R_K}\frac{\exp(-iwt)}{1-\exp\left(-\frac{\hbar\omega}{2k_BT_{\mathrm{env}}}\right)} = \tag{5.3}$$

$$2\int_{0}^{\infty}\frac{d\omega}{\omega}\frac{\mathrm{Re}[Z_t(\omega)]}{R_K}\left\{\coth\left(\frac{\hbar\omega}{2k_BT_{\mathrm{env}}}\right)[\cos(\omega t)-1] - i\sin(\omega t)\right\}, \tag{5.4}$$

where T_{env} is the temperature of the environment, $R_K = h/e^2$ is the resistance quantum, and ω is angular frequency. The probability follows the detailed balance condition $P(-E) = \exp(-E/k_BT)P(E)$ indicating that exciting photons is a more likely event than absorbing them and that when temperature is zero no energy can be absorbed [44].

When $\mathrm{Re}[Z_t] \ll R_K$ the quantum fluctuations are small and can be ignored. Then $J(t)$ becomes

$$J(t) = \frac{2\pi}{R_K\hbar}\int_0^{\infty} d\omega\frac{S_V(\omega)}{\omega^2}[\cos(\omega t)-1], \tag{5.5}$$

where

$$S_V(\omega) = \frac{2}{\pi}\frac{\mathrm{Re}[Z_t(\omega)]\hbar\omega}{\exp(\hbar\omega/k_BT)-1}. \tag{5.6}$$

is Planck radiation formula for voltage noise of impedance Z_t. When this noise is only weakly coupled to the tunnel junctions, equation (5.2) can be expanded to the first order in $J(t)$, yielding

$$P(E) = \frac{1}{2\pi\hbar}\int_{-\infty}^{\infty} dt e^{iEt/\hbar}[1+J(t)] = \tag{5.7}$$

$$= \frac{1}{2\hbar}\delta(E) + \frac{\pi S_V(E/\hbar)}{R_KE^2}, \tag{5.8}$$

where we have used the fact that Fourier transforms of 1 and cosine are delta-functions. The latter part is valid at energies $E \neq 0$.

In Publication IV equation (5.8) was used. However, the exact form for $Z_t(\omega)$ was hard to calculate and some approximations were needed. First the voltage

noise at the radiation source was assumed to have the form of thermal radiation in free space,

$$S_V(\omega) = \frac{\hbar\omega^3}{4\pi^3 c^2} \frac{1}{\exp(\hbar\omega/k_B T) - 1}. \tag{5.9}$$

where T is the temperature of the noise source. One should note that in our context this is only a crude approximation since in order to reach the sample the signal has already penetrated through sample stage shields and/or signal line filters. In addition, in a realistic case the noise does not originate from single point at fixed temperature but the temperature of the radiation depends on cryostat geometry. Therefore equation (5.9) should be considered only as a phenomenological model.

The filters are included in equation (5.8) as an attenuation term $\kappa(\omega)$ and the noise at the detector is modelled as $S_{V,\mathrm{DET}} = \kappa(\omega) S_V$. The attenuation was calculated based on telegrapher's equations for lossy transmission lines. Since we anyway used a phenomenological model for the noise spectrum, we neglect reflections at the detector for simplicity. Different attenuation components were assumed to be additive. This led to an approximation

$$\kappa(\omega, B, T) = \kappa_{\mathrm{JAF}}(\omega, B)\kappa_{\mathrm{RCF}}(\omega, T) + \kappa_0, \tag{5.10}$$

where $\kappa_{\mathrm{JAF}}(\omega, B)$ and $\kappa_{\mathrm{RCF}}(\omega, T)$ are the attenuations caused by the magnetic field dependent SQUID array filter and temperature dependent capacitive shunt filter, respectively. These filters have been discussed in more detail in section 3.1.2. Not all the lines (for example, the gate line with voltage V_g) were filtered and some noise traveled to the detector also through these channels bypassing the other filters. Term κ_0 describes this channel. Model of equation (3.1.2) yielded a reasonable good agreement with the experimental data.

5.2 SINIS cooler with phonon transport limited heat flow

In Publication V we used semiconductor–superconductor (Sm-S) tunnel junctions [92] to cool mm-scale suspended silicon chips, called sub-chips (see figure 5.3). These junctions were analogous to NIS junctions and followed the theory introduced in section 2.1. NIS junction coolers (and their SmS counterparts) [31, 32, 33] as well as other solid state electrical coolers have been studied before [25, 26, 27, 28, 29, 30, 93, 94], since many devices [95, 96, 97, 98, 99] require sub kelvin temperatures that can be reached only by massive and expensive cryo-liquid based equipment. Solid state coolers would thus make the refrigeration more compact and less expensive.

At the moment, temperatures of 1 K ... 4 K can be reached using ^{4}He based cryocoolers. Helium-4 boils at 4.2 K at atmospheric pressure and the temperature can be brought further down by using pulse tube based cryocoolers (3 K) or by pumping it continuously to lower the pressure (down to 1 K). However, cooling below these temperatures requires the use of ^{3}He, which increases the

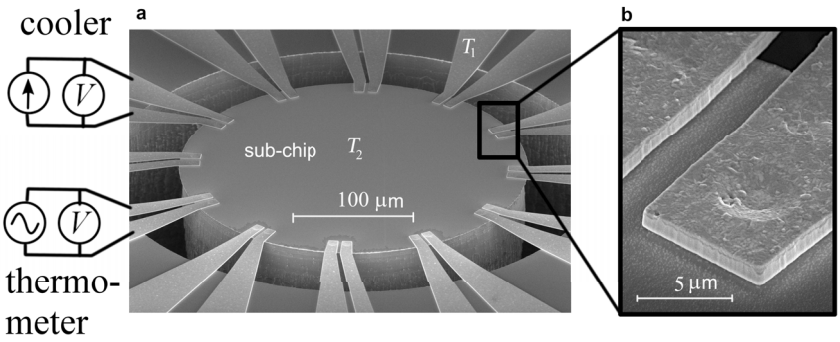

Figure 5.3. a)-b) Scanning electron micrographs of the samples studied in Publication V. a) Simplified measurement setup. b) Two pieces of aluminium leads.

costs considerably. With ^{3}He one can reach 300 mK with similar low pressure methods as with ^{4}He and temperatures of a few millikelvin are reachable by utilizing the mixing properties of ^{3}He and ^{4}He. However, the coolers based on mixing of ^{3}He and ^{4}He need another cryocooler to keep the mixture liquefied, which increases complexity. Natural first goal for the electric low temperature coolers would thus be that they could replace the ^{3}He based devices and cool down from the operation temperatures of the ^{4}He cryocoolers. It should also be noted that the background temperature of space is about 3 K, but many spaceborne detectors need sub kelvin temperatures [99].

Presently, maybe the best results at sub-K temperatures have been achieved with NIS junctions, though no cooler has yet emerged that could cover large enough temperature range. The refrigeration of NIS coolers is based on electrically cooling the normal metal part of the device, which is traditionally connected to the payload with cold fingers. The heat leaks that limit the cooling in these devices have usually been mediated by the electron-phonon interaction in the normal metal part of NIS junction and by its phonon-phonon thermalization to substrate (see section 2.1.3). The best results obtained with NIS coolers so far include refrigeration of a transition edge sensor on a SiN membrane by 110 mK [31], a cube with the volume 0.16 mm^3 by 95 mK [32], and a 1.9 cm^3 copper stage by 34 mK [33], all starting from about 300 mK.

In Publication V we introduced a different sample scheme as shown in figures 5.3 and 5.4. Here the Sm-S tunnel junctions are fabricated at the interface between aluminium leads and silicon sub-chip and they function as both: electric coolers and phonon heat barriers. Therefore no cold fingers are needed. The normal metal part of the junctions, i.e. the sub-chip, is connected to the substrate only through the aluminium leads, and majority of the heat that enters the sub-chip flows through the Sm-S interface and the leads. The performance of our junctions is typical for thermionic refrigerators [100], where energetic electrons are ejected through vacuum or solid barrier and phonon transport is suppressed by the same barrier.

We observed (see figure 5.5a) that the thermal conductance from the sub-chip

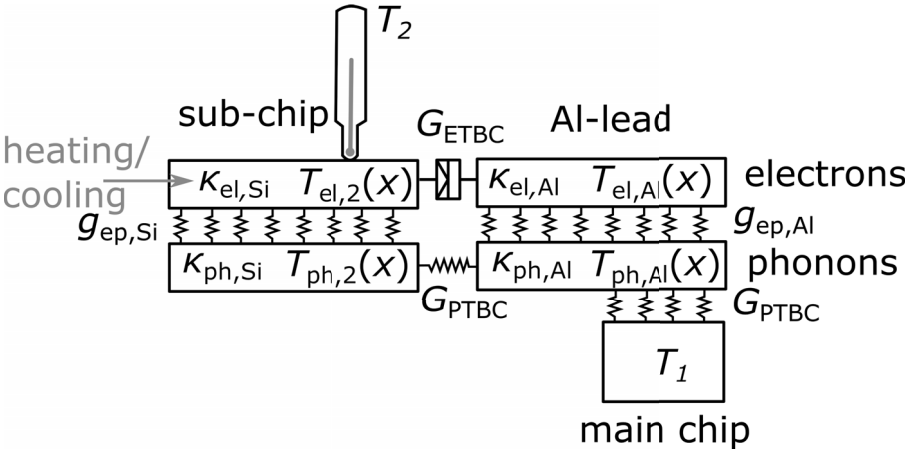

Figure 5.4. Heat model of the samples studied in Publication V. The model introduces the electron and phonon thermal conductivities at the sub-chip ($\kappa_{el,Si}$ and $\kappa_{ph,Si}$, respectively) and at the aluminium leads ($\kappa_{el,Al}$ and $\kappa_{ph,Al}$, respectively) in addition to the electron and phonon thermal boundary conductances (G_{ETBC}, G_{PTBC}, respectively). Due to the large size of the sub-chip, electrons and phonons in it share the same temperature $T_{el,2} = T_{el,2} = T_2$. This is not the case in aluminium leads.

to the environment has a T^3 dependence, which is typical for both: the phonon thermal conductance at the Sm-S junction interface and the phonon conductance of the aluminium leads. These were concluded to be the main heat channels in our devices. This was due, in addition to the mechanisms mentioned above, to the facts that the electric heat leaks through the Sm-S interface were suppressed by the NIS junction and that superconductivity suppressed the coupling between electrons and phonons in the aluminium leads. Also the large size and high dopant concentration of the sub-chip played a role, since they ensured that electron and phonons were at the same temperature in the sub-chip.

In Publication V we demonstrated refrigeration of 83 mK starting from 244 mK (see figure 5.5b) or 40 % at 170 mK. In addition, we showed by simulations that in aluminium the refrigeration can be improved to over 80 % simply by decreasing junction resistance and leakage in the superconducting energy gap by realistic amounts [85], see figure 5.5c. Maybe even more importantly, we showed, by simulation that enhancing the phonon blocking at the interface can have only minor effect on the overall performance. This means that the phonon heat bottlenecks are already sufficient for Al-Si based coolers.

On the other hand, the performance of our coolers was still modest compared to that needed to replace any of the cryo-liquid based cooling steps. To increase the temperature range of Sm-S (or NIS) based coolers, cascading junctions that have different superconductors is a must. From figure 5.5c we see that in contrary to Al-Si based coolers devices with higher T_c could benefit from phonon engineering methodologies. This is a topic widely studied, since it could improve e.g. the performance of thermoelectric coolers, energy harvesters and nanoscale electronics [101, 102]. In Publication V we analyzed, through simulation, that starting temperature of about 1.5 K could be possible utilizing a vanadium-

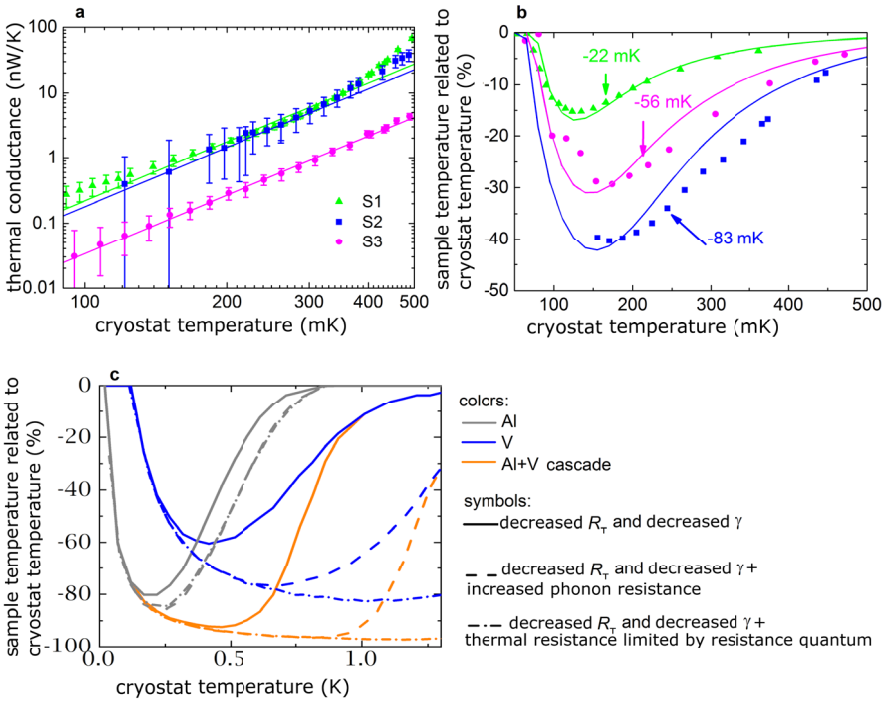

Figure 5.5. a) Measured thermal conductance between sub-chip and environment (squares, dots and circles) as a function of cryostat temperature (i.e. the environmental temperature) for three different samples with different sub-chips. The lines correspond to power law of the form T^3 b) The relative temperature decrease related to cryostat temperature (squares, dots and circles). The arrows indicate the maximum absolute temperature reduction. The lines correspond to simulations utilizing the prefactors of the T^3 polynomials obtained from a, sample parameters obtained from IV characterizations and cooling power obtained from equation (2.17) c) Simulations with improved electric and phononic characteristics for aluminium (gray) and vanadium (blue) based coolers and for a cascaded cooler utilizing both Al-Si and V-Si junctions (orange). All simulations contain improved electric characteristics (junction resistance and quality). However, the solid lines present a situation, where the phonon heat bottlenecks are the same as in figure a, whereas the dashed lines show the cooling when the overall thermal conductance between sub-chip and environment is decreased tenfold. Finally, in simulations presented by the dash dotted lines, the phonon thermal conductance is replaced with constant number of conductance quanta.

silicon and an aluminium-silicon stage (see figure 5.5c). Vanadium was chosen as the high-T superconductor, as it has suitable temperature range and it has shown promising cooler behavior [103]. We considered two different scenarios: when the thermal conductance is decreased to one tenth of its original value due to, for example by introducing nanowire constrictions in the aluminium line, and the conductance quantum limit. These simulations ignored quasiparticle effects but further simulations (see supplementary information of Publication V) showed that cooling from 1.5 K down to few hundred millikelvins is still viable using two V-Si and two Al-Si stages.

6. Summary

This thesis explored ways to create measurement standards for the kelvin and the ampere. It also studied devices which were byproducts of this research and enablers for it.

We studied Coulomb blockade thermometer as a potential realization of the kelvin in the temperature range from 20 mK to 200 mK. We constructed a traceable measurement setup, where the temperature could be determined with the help of Boltzmann constant and traceable voltage measurements. In addition, we compared CBT against the PLTS-2000 temperature scale (Publication II), and against two other primary thermometers that were also based on Boltzmann constant (Publication III).

During this thesis, we observed quantum phase slips in a novel material: molybdenium silicide (MoSi, Publication VI). If the QPS events are coherent they can be used to produce a quantum standard for the ampere. Our sample layout, which was used for these first material tests, could not be used to indicate coherence. However, it is commonly believed that high normal state resistivity is needed to enable it, and the resistivity of MoSi can be easily tuned with rapid thermal annealing making it a promising material.

SINIS turnstiles were studied during this thesis as potential realizations of the ampere. We observed quasiparticle effects in SINIS devices that deviated from thermal models. However, no model to explain these effects were found. In addition, parallelized SINIS devices were fabricated, but sample fabrication problems destroyed the accuracy of their output current.

It has been speculated whether the small output signals of quantum current standards can be brought to room temperature with low enough noise, since long cables are needed to transfer the signal: In all modern cryostats, and especially in those driven by pulse tube precooler, vibration induced current noise can change the required averaging times from hours to weeks. However, in Publication I we demonstrated cable assembly including vacuum insulated cables that guaranteed low noise even in pulse tube based cryostats.

Filtering the high frequency noise is important, since the noise photons can have enough energy to break Cooper pairs or cause unwanted tunnelings. In Publication IV we studied two different tunable filters: capacitive shunt super-

conducting transmission line filter and superconducting quantum interference device (SQUID). Surprisingly, we observed that superconductivity can play a role in signal transmission even at frequencies which are greater than those needed to break Cooper pairs. In addition, we characterized a SQUID-based filter in low noise environment and at frequency range starting from 50 GHz and extending up to 200 GHz. The noise environment was such which can also be found in actual measurement setups.

Last but not least, Publication V demonstrated cooling with semiconductor-superconductor (Sm-S) tunnel junctions. In addition, the measurements were performed in a novel geometry: Usually the refrigeration, enabled by these devices, is limited by heat flow due to electron-phonon coupling. Here, however, the main heat transport channels were the phonon thermal boundary conductance of Sm-S junction and that of the aluminium leads. Not only could the measurements demonstrate cooling of macroscopic (mm-scale) silicon chip in this geometry, they also showed that the thermal conductance of Sm-S junctions follows theoretical values. In Publication V we also analyzed the possibilities to extend the cooling from 100 mK... 300 mK regime to higher temperatures by cascading coolers and utilizing superconductors with higher critical currents. Our simulations indicate that electrical cooling from 1.5 K to 100 mK is a realistic goal. Such refrigerators would be beneficial for example in quantum and space technologies.

References

[1] Bureau International des Poids et Mesures, "The international system of units (SI)," *Stedi Media, Paris, 8th edition*, 2006.

[2] Information on the redifinition of the SI can be found e.g. here: https://www.bipm.org/utils/common/pdf/SI-statement.pdf and here https://www.bipm.org/en/measurement-units/rev-si/.

[3] M. J. T. Milton, R. Davis, and N. Fletcher, "Toward a new SI: a review of progress made since 2011," *Metrologia*, vol. 51, pp. R21–R30, 2014.

[4] J. P. Pekola, K. P. Hirvi, J. P. Kauppinen, and M. A. Paalanen, "Thermometry by arrays of tunnel junctions," *Physical Review Letters*, vol. 73, pp. 2903–2906, Nov 1994.

[5] J. P. Pekola, J. J. Vartiainen, M. Möttönen, S. O.-P., M. M., and A. D. V, "Hybrid single-electron transistor as a source of quantized electric current," *Nature Physics*, vol. 4, p. 120, 2008.

[6] B. Josephson, "Possible new effects in superconductive tunnelling," *Physics Letters*, vol. 1, no. 7, pp. 251 – 253, 1962.

[7] J. E. Mooij and Y. V. Nazarov, "Superconducting nanowires as quantum phase-slip junctions," *Nature Physics*, vol. 2, pp. 169–172, 2006.

[8] J.-S. Tsai, A. K. Jain, and J. E. Lukens, "High-precision test of the universality of the josephson voltage-frequency relation," *Phys. Rev. Lett.*, vol. 51, pp. 316–319, Jul 1983.

[9] H. Preston-Thomas, "The international temperature scale of 1990 (ITS-90)," *Metrologia*, vol. 27, no. 1, p. 3, 1990.

[10] R. L. Rusby, M. Durieux, A. L. Reesink, R. P. Hudson, G. Schuster, M. Kühne, W. E. Fogle, R. J. Soulen, and E. D. Adams, "The provisional low temperature scale from 0.9 mK to 1 K, PLTS-2000," *Journal of Low Temperature Physics*, vol. 126, pp. 633–642, Jan 2002.

[11] A. Kirste and J. Engert, "A SQUID-based primary noise thermometer for low-temperature metrology.," *Philosophical transactions of the royal society A. Mathematical, physical and engineering sciences.*, vol. 374, p. 20150050, 2016.

[12] A. Schibahara, O. Hahtela, J. Engert, H. van der Vliet, L. V. Levitin, A. Casey, C. P. Lusher, J. Saunders, D. Drung, and T. Schuriq, "Primary current-sensing noise thermometry in millikelvin regime," *Philosophical transactions of the royal society A. Mathematical, physical and engineering sciences.*, vol. 374, p. 20150054, 2016.

[13] D. I. Bradley, R. E. George, D. Gunnarsson, R. P. Haley, H. Heikkinen, Y. A. Pashkin, J. Penttilä, J. R. Prance, M. Prunnila, L. Roschier, and M. Sarsby, "Nanoelectric primary thermometry below 4 mK," *Nature Communications*, 2016.

[14] M. Meschke, A. Kemppinen, and J. P. Pekola, "Accurate Coulomb blockade thermometry up to 60 K," *Philosophical transactions of the royal society A. Mathematical, physical and engineering sciences.*, vol. 374, p. 20150052, 2016.

[15] J. P. Pekola, O.-P. Saira, V. F. Maisi, A. Kemppinen, M. Möttönen, Y. A. Pashkin, and D. V. Averin, "Single-electron current sources: Toward a refined definition of the ampere," *Reviews of Modern Physics*, vol. 85, pp. 1421–1472, Oct 2013.

[16] Bureau International des Poids et Mesures, "The international system of units (SI), appendix 2," *Stedi Media, Paris, 8th edition*, 2018. Available only online: https://www.bipm.org/en/publications/mises-en-pratique/electrical-units.html.

[17] S. Shapiro, "Josephson currents in superconducting tunneling: The effect of microwaves and other observations," *Phys. Rev. Lett.*, vol. 11, pp. 80–82, Jul 1963.

[18] K. v. Klitzing, G. Dorda, and M. Pepper, "New method for high-accuracy determination of the fine-structure constant based on quantized Hall resistance," *Physical Review Letters*, vol. 45, pp. 494–497, Aug 1980.

[19] B. M. Wood and S. Solve, "A review of josephson comparison results," *Metrologia*, vol. 46, no. 6, p. R13, 2009.

[20] T. J. B. M. Janssen, N. E. Fletcher, R. Goebel, J. M. Williams, A. Tzalenchuk, R. Yakimova, S. Kubatkin, S. Lara-Avila, and V. I. Falko, "Graphene, universality of the quantum Hall effect and redefinition of the SI system," *New Journal of Physics*, vol. 13, no. 9, p. 093026, 2011.

[21] A. Hartland, K. Jones, J. M. Williams, B. L. Gallagher, and T. Galloway, "Direct comparison of the quantized hall resistance in gallium arsenide and silicon," *Phys. Rev. Lett.*, vol. 66, pp. 969–973, Feb 1991.

[22] N. Feltin and F. Piquemal, "Determination of the elementary charge and the quantum metrological triangle experiment," *The European Physical Journal Special Topics*, vol. 172, pp. 267–296, Jun 2009.

[23] F. Stein, H. Scherer, T. Gerster, R. Behr, M. Götz, E. Pesel, C. Leicht, N. Ubbelohde, T. Weimann, K. Pierz, H. W. Schumacher, and F. Hohls, "Robustness of single-electron pumps at sub-ppm current accuracy level," *Metrologia*, vol. 54, no. 1, p. S1, 2017.

[24] G. Yamahata, S. P. Giblin, M. Kataoka, T. Karasawa, and A. Fujiwara, "Gigahertz single-electron pumping in silicon with an accuracy better than 9.2 parts in 10^7," *Applied Physics Letters*, vol. 109, no. 1, p. 013101, 2016.

[25] J. R. Prance, C. G. Smith, J. P. Griffiths, S. J. Chorley, D. Anderson, G. A. C. Jones, I. Farrer, and D. A. Ritchie, "Electronic refrigeration of a two-dimensional electron gas," *Phys. Rev. Lett.*, vol. 102, p. 146602, Apr 2009.

[26] J. Rossnagel, S. T. Dawkins, K. N. Tolazzi, A. Obinna, E. Lutz, F. Schmidt-Kaler, and K. Singer, "A single-atom heat engine," *Science*, vol. 352, pp. 325–329, 2016.

[27] S. Whalen, M. Thompson, D. Bahr, C. Richards, and R. Richards, "Design, fabrication and testing of the p3 micro heat engine," *Sensors and Actuators A: Physical*, vol. 104, no. 3, pp. 290 – 298, 2003.

[28] P. G. Steeneken, K. Le Phan, M. J. Goossens, G. E. J. Koops, G. J. A. M. Brom, C. van der Avoort, and J. T. M. van Beek, "Piezoresistive heat engine and refrigerator," *Nature Physics*, vol. 7, pp. 354–, Jan. 2011.

[29] J.-P. Bratut, G. Grenier, J. Meineke, D. Stadler, S. Krinner, C. Kollath, T. Esslinger, and A. Georges, "A thermoelectric heat engine with ultracold atoms," *Science*, vol. 342, no. 6159, pp. 713–715, 2013.

[30] A. V. Feshchenko, J. V. Koski, and J. P. Pekola, "Experimental realization of a Coulomb blockade refrigerator," *Physical Review B*, vol. 90, p. 201407, Nov 2014.

[31] N. A. Miller, G. C. O'Neill, J. A. Beall, G. C. Hilton, K. D. Irwin, D. R. Schmidt, L. R. Vale, and J. N. Ullom, "High resolution x-ray transtion-edge sensor cooled by tunnel junction refrigerators," *Applied Physics Letters*, vol. 92, p. 163501, 2008.

[32] A. M. Clark and N. A. Miller, "Cooling of bulk material by electron-tunneling refrigerators," *Applied Physics Letters*, vol. 86, p. 173508, 2005.

[33] P. J. Lowell, G. C. O'Neill, J. M. Underwood, and J. N. Ullom, "Macroscale refrigeration by nanoscale electron transport," *Applied Physics Letters*, vol. 102, p. 082601, 2013.

[34] O.-P. Saira, A. Kemppinen, V. F. Maisi, and J. P. Pekola, "Vanishing quasiparticle density in hybrid Al/Cu/Al single-electron transistor," *Physical Review B*, vol. 85, no. 1, p. 012504, 2012.

[35] R. Barends, J. Wenner, M. Lenander, Y. Chen, R. C. Bialczak, J. Kelly, E. Lucero, P. O'Malley, M. Mariantoni, D. Sank, H. Wang, T. C. White, Y. Yin, J. Zhao, A. N. Cleland, J. M. Martinis, and J. J. A. Baselmans, "Minimizing quasiparticle generation from stray infrared light in superconducting quantum circuits," *Applied Physics Letters*, vol. 99, p. 113507, 2011.

[36] A. D. Corcoles, J. M. Chow, J. M. Gambetta, C. Rigetti, J. R. Rozen, G. A. Keefe, M. Beth Rothwell, M. B. Ketchen, and M. Steffen, "Protecting superconducting qubits from radiation," *Applied Physics Letters*, vol. 99, no. 18, p. 181906, 2011.

[37] P. J. de Visser, J. J. A. Baselmans, S. J. C. Yates, P. Diener, A. Endo, and T. M. Klapwijk, "Microwave-induced excess quasiparticles in superconducting resonators measured through correlated conductivity fluctuations," *Applied Physics Letters*, vol. 100, no. 16, p. 162601, 2012.

[38] J. P. Pekola, V. F. Maisi, S. Kafanov, N. Chekurov, A. Kemppinen, Y. A. Pashkin, O.-P. Saira, M. Möttönen, and J. S. Tsai, "Environment-assisted tunneling as an origin of the Dynes density of states," *Physical Review Letters*, vol. 105, p. 026803, Jul 2010.

[39] A. Kemppinen, S. V. Lotkhov, O.-P. Saira, A. B. Zorin, J. P. Pekola, and A. J. Manninen, "Long hold times in a two-junction electron trap," *Applied Physics Letters*, vol. 99, no. 14, p. 142106, 2011.

[40] S. V. Lotkhov, A. Kemppinen, S. Kafanov, J. P. Pekola, and A. B. Zorin, "Pumping properties of the hybrid single-electron transistor in dissipative environment," *Applied Physics Letters*, vol. 95, no. 11, p. 112507, 2009.

[41] S. V. Lotkhov and A. B. Zorin, "A hybrid superconductor-normal metal electron trap as photon detector," *Applied Physics Letters*, vol. 100, p. 242601, 2012.

[42] S. V. Lotkhov, O.-P. Saira, J. P. Pekola, and A. B. Zorin, "Single-charge escape processes through a hybrid turnstile in dissipative environment," *New Journal of Physics*, vol. 13, p. 013040, 2011.

[43] S. V. Lotkhov, B. Jalali-Jafari, and A. B. Zorin, "Photon-activated electron hopping in a single-electron trap enhanced by Josephson radiation," *Applied Physics Letters*, vol. 108, p. 172603, 2016.

[44] G. L. Ingold and Y. V. Nazarov, *Single charge tunneling*, vol. 294. Plenum Press, New York, 1992.

[45] K. Gloos, P. J. Koppinen, and J. P. Pekola, "Properties of native ultrathin aluminium oxide tunnel barriers," *Journal of Physics: Condensed Matter*, vol. 15, no. 10, p. 1733, 2003.

[46] M. Tinkham, *Introduction to superconductivity*. MacGraw-Hill, Inc, 1996.

[47] R. C. Dynes, V. Narayanamurti, and J. P. Garno, "Direct measurement of quasiparticle-lifetime broadening in a strong-coupled superconductor," *Physical Review Letters*, vol. 41, pp. 1509–1512, Nov 1978.

[48] R. C. Dynes, J. P. Garno, G. B. Hertel, and T. P. Orlando, "Tunneling study of superconductivity near the metal-insulator transition," *Physical Review Letters*, vol. 53, pp. 2437–2440, Dec 1984.

[49] D. V. Averin and K. Likharev, "Coulomb blockade of single-electron tunneling, and coherent oscillations in small tunnel junctions," *Journal of Low Temperature Physics*, vol. 62, p. 345, 1986.

[50] K. Likharev, "Single-electron transistors: Electrostatic analogs of the dc SQUIDS," *IEEE Transactions on Magnetics*, vol. 23, no. 2, p. 1142, 1987.

[51] T. A. Fulton and G. J. Dolan, "Observation of single-electron charging effects in small tunnel junctions," *Phys. Rev. Lett.*, vol. 59, pp. 109–112, Jul 1987.

[52] E. Mykkänen, "Traceable measurement for a quantum current source," Master's thesis, Aalto University, School of Techonogy, 2013.

[53] F. Giazotto, T. T. Heikkilä, A. Luukanen, A. M. Savin, and J. P. Pekola, "Opportunities for mesoscopics in thermometry and refrigeration: Physics and applications," *Reviews of Modern Physics*, vol. 78, pp. 217–274, Mar 2006.

[54] M. M. Leivo, J. P. Pekola, and A. D. V, "Efficient Peltier refrigeration by a pair of normal metal/insulator/superconductor junctions," *Applied Physics Letters*, vol. 68, p. 1996, 1996.

[55] H. S. Knowles, V. F. Maisi, and J. P. Pekola, "Probing quasiparticle excitations in a hybrid single electron transistor," *Applied Physics Letters*, vol. 100, p. 262601, 2012.

[56] A. V. Timofeev, C. P. García, N. B. Kopnin, A. M. Savin, M. Meschke, F. Giazotto, and J. P. Pekola, "Recombination-limited energy relaxation in a bardeen-cooper-schrieffer superconductor," *Phys. Rev. Lett.*, vol. 102, p. 017003, Jan 2009.

[57] D. E. McCumber and B. I. Halperin, "Time scale of intrinsic resistive fluctuations in thin superconducting wires," *Phys. Rev. B*, vol. 1, pp. 1054–1070, Feb 1970.

[58] N. Giordano, "Evidence for macroscopic quantum tunneling in one-dimensional superconductors," *Phys. Rev. Lett.*, vol. 61, pp. 2137–2140, Oct 1988.

[59] N. Giordano and E. R. Schuler, "Macroscopic quantum tunneling and related effects in a one-dimensional superconductor," *Phys. Rev. Lett.*, vol. 63, pp. 2417–2420, Nov 1989.

[60] F. Sharifi, A. V. Herzog, and R. C. Dynes, "Crossover from two to one dimension in in situ grown wires of pb," *Phys. Rev. Lett.*, vol. 71, pp. 428–431, Jul 1993.

[61] A. Bezryadin, C. N. Lau, and M. Tinkham, "Quantum supression of superconductivity in ultrathin nanowires," *Nature*, vol. 404, pp. 971–974, 2000.

[62] C. N. Lau, N. Markovic, M. Bockrath, A. Bezryadin, and M. Tinkham, "Quantum phase slips in superconducting nanowires," *Phys. Rev. Lett.*, vol. 87, p. 217003, Nov 2001.

[63] M. Zgirski, K.-P. Riikonen, V. Touboltsev, and K. Y. Arutyunov, "Quantum fluctuations in ultranarrow superconducting aluminum nanowires," *Phys. Rev. B*, vol. 77, p. 054508, Feb 2008.

[64] A. D. Zaikin, D. S. Golubev, A. van Otterlo, and G. T. Zimányi, "Quantum phase slips and transport in ultrathin superconducting wires," *Phys. Rev. Lett.*, vol. 78, pp. 1552–1555, Feb 1997.

[65] D. S. Golubev and A. D. Zaikin, "Quantum tunneling of the order parameter in superconducting nanowires," *Phys. Rev. B*, vol. 64, p. 014504, Jun 2001.

[66] K. Uhlig, "^{3}He/^{4}He dilution refrigerator with pulse-tube refrigerator precooling," *Cryogenics*, vol. 42, pp. 73–77, 2002.

[67] R. Kalra, A. Laucht, J. P. Dehollain, D. Bar, S. Freer, S. Simmons, J. T. Muhonen, and A. Morello, "Vibration-induced electrical noise in a cryogen-free dilution refrigerator: Characterization, mitigation, and impact on qubit coherence," *Review of Scientific Instruments*, vol. 87, p. 073905, 2016.

[68] D. Drung, C. Krause, S. P. Giblin, S. Djordjevic, F. Piquemal, O. Seron, F. Rengnez, M. Götz, E. Pesel, and H. Scherer, "Validation of the ultrastable low-noise current amplifier as travelling standard for small direct currents," *Metrologia*, vol. 6, no. 52, pp. 756–763, 2015.

[69] D. Drung, C. Krause, U. Becker, H. Scherer, and F. J. Ahlers, "Ultrastable low-noise current amplifier: A novel device for measuring small electric currents with high accuracy," *Review of Scientific Instruments*, vol. 86, no. 2, 2015.

[70] D. Drung, M. Götz, E. Pesel, and H. Scherer, "Improving the traceable measurement and generation of small direct currents," *IEEE Transactions on Instrumentation and Measurement*, vol. 64, pp. 3021–3030, Nov 2015.

[71] A. Lukashenko and A. V. Ustinov, "Improved powder filters for qubit measurements," *Review of Scientific Instruments*, vol. 79, p. 014701, 2008.

[72] A. B. Zorin, "The thermocoax cable as the microwave frequency filter for single electron circuits," *Review of Scientific Instruments*, vol. 66, p. 4296, May 1995.

[73] S. Corlevi, W. Guichard, F. W. J. Hekking, and D. B. Haviland, "Coulomb blockade of Cooper pair tunneling and parity effects in the Cooper pair transistor," *Physical Review B*, vol. 74, p. 224505, Dec 2006.

[74] M. Watanabe and D. B. Haviland, "Coulomb blockade and coherent single-Cooper-pair tunneling in single Josephson junctions," *Physical Review Letters*, vol. 86, pp. 5120–5123, May 2001.

[75] O. V. Astafiev, I. B. Ioffe, S. Kafanov, Y. A. Pashkin, K. Y. Arutyunov, S. D., O. Cohen, and J. S. Tsai, "Coherent quantum phase slip," *Nature*, vol. 484, pp. 355–358, 2012.

[76] T. T. Hongisto and A. B. Zorin, "Single-charge transistor based on the charge-phase duality of a superconducting nanowire circuit," *Phys. Rev. Lett.*, vol. 108, p. 097001, Feb 2012.

[77] S. E. de Graaf, S. T. Skacel, T. Hönigl-Decrinis, R. Shaikhaidarov, H. Rotzinger, S. Linzen, M. Ziegler, U. Hübner, H.-G. Meyer, V. Antonov, E. Il'ichev, A. V. Ustinov, A. Y. Tzalenchuk, and O. V. Astafiev, "Charge quantum interference device," *Nature Physics*, vol. 14, no. 6, pp. 590–594, 2018.

[78] S. Kafanov and N. M. Chtchelkatchev, "Single flux transistor: The controllable interplay of coherent quantum phase slip and flux quantization," *Journal of Applied Physics*, vol. 114, no. 7, p. 073907, 2013.

[79] J. S. Lehtinen, K. Zakharov, and K. Y. Arutyunov, "Coulomb blockade and bloch oscillations in superconducting Ti nanowires," *Physical Review Letters*, vol. 109, p. 187001, Oct 2012.

[80] A. Di Marco, F. W. J. Hekking, and G. Rastelli, "Quantum phase-slip junction under microwave irradiation," *Phys. Rev. B*, vol. 91, p. 184512, May 2015.

[81] C. H. Webster, J. C. Fenton, T. T. Hongisto, S. P. Giblin, A. B. Zorin, and P. A. Warburton, "Nbsi nanowire quantum phase-slip circuits: dc supercurrent blockade, microwave measurements, and thermal analysis," *Physical Review B*, vol. 87, p. 144510, Apr 2013.

[82] K. Cedergren, R. Ackroyd, S. Kafanov, N. Vogt, A. Shnirman, and T. Duty, "Insulating josephson junction chains as pinned luttinger liquids," *Physical Review Letters*, vol. 119, p. 167701, Oct 2017.

[83] D. V. Averin and J. P. Pekola, "Nonadiabatic charge pumping in a hybrid single-electron transistor," *Physical Review Letters*, vol. 101, p. 066801, Aug 2008.

[84] J. P. Pekola, T. T. Heikkilä, A. M. Savin, J. T. Flyktman, F. Giazotto, and F. W. J. Hekking, "Limitations in cooling electrons using normal-metal-superconductor tunnel junctions," *Physical Review Letters*, vol. 92, p. 056804, Feb 2004.

[85] D. Gunnarsson, J. S. Richardson-Bullock, M. J. Prest, H. Q. Nguyen, A. V. Timoveef, V. A. Shah, T. E. Whall, E. H. C. Parker, M. Myronov, and M. Prunnila, "Interfacial engineering of semiconductor-superconductor junctions for high performance micro-coolers," *Scientific Reports*, vol. 5, p. 17398, 2015.

[86] J. T. Peltonen, A. Moisio, V. F. Maisi, M. Meschke, J. S. Tsai, and J. P. Pekola, "Hybrid single-electron turnstiles with thick superconducting electrodes for improved quasiparticle relaxation," *arXiv:1709.09832*, 2017.

[87] V. F. Maisi, O.-P. Saira, Y. A. Pashkin, J. S. Tsai, D. V. Averin, and J. P. Pekola, "Real-time observation of discrete andreev tunneling events," *Phys. Rev. Lett.*, vol. 106, p. 217003, May 2011.

[88] S. P. Giblin, M. Kataoka, N. Fletcher, P. See, T. J. B. M. Janssen, J. P. Griffiths, G. A. C. Jones, I. Farrer, and D. A. Ritchie, "Towards a quantum representation of the ampere using single electron pumps," *Nature Communications*, vol. 3, p. 930, 2012.

[89] O.-P. Saira, *Electrostatic control of quasiparticle transport in superconducting hybrid nanostructures*. PhD thesis, Aalto University, School of Techonogy, 2013.

[90] B. Fellmuth, J. Fischer, G. Machin, S. Picard, P. P. M. Steur, O. Tamura, D. R. White, and H. Yoon, "The kelvin redefinition and its mise en pratique," *Philosophical Transactions of the Royal Society of London A: Mathematical, Physical and Engineering Sciences*, vol. 374, no. 2064, 2016.

[91] G. Machin, "The kelvin redefined," *Measurement Science and Technology*, vol. 29, no. 2, p. 022001, 2018.

[92] A. M. Savin, M. Prunnila, P. P. Kivinen, J. P. Pekola, J. Ahopelto, and A. J. Manninen, "Efficient electronic cooling in heavily doped silicon by quasiparticle tunneling," *Applied Physics Letters*, vol. 79, no. 10, pp. 1471–1473, 2001.

[93] D. I. Bradley, A. M. Guénault, D. Gunnarsson, R. P. Haley, S. Holt, A. T. Jones, Y. A. Pashkin, J. Penttilä, J. R. Prance, M. Prunnila, and L. Roschier, "On-chip magnetic cooling of a nanoelectronic device," *Scientific Reports*, vol. 7, pp. 45566–, Apr. 2017.

[94] C. Ciccarelli, R. P. Campion, B. L. Gallagher, and A. J. Ferguson, "Intrinsic magnetic refrigeration of a single electron transistor," *Applied Physics Letters*, vol. 108, no. 5, p. 053103, 2016.

[95] J. Kelly, R. Barends, A. G. Fowler, A. Megrant, E. Jeffrey, T. C. White, D. Sank, J. Y. Mutus, B. Campbell, Y. Chen, Z. Chen, B. Chiaro, A. Dunsworth, I.-C. Hoi, C. Neill, P. J. J. O'Malley, C. Quintana, P. Roushan, A. Vainsencher, J. Wenner, A. N. Cleland, and J. M. Martinis, "State preservation by repetitive error detection in a superconducting quantum circuit," *Nature*, vol. 519, pp. 66–, Mar. 2015.

[96] M. W. Johnson, M. H. S. Amin, S. Gildert, T. Lanting, F. Hamze, N. Dickson, R. Harris, A. J. Berkley, J. Johansson, P. Bunyk, E. M. Chapple, C. Enderud, J. P. Hilton, K. Karimi, E. Ladizinsky, N. Ladizinsky, T. Oh, I. Perminov, C. Rich, M. C. Thom, E. Tolkacheva, C. J. S. Truncik, S. Uchaikin, J. Wang, B. Wilson, and G. Rose, "Quantum annealing with manufactured spins," *Nature*, vol. 473, pp. 194–, May 2011.

[97] C. M. Natarajan, M. G. Tanner, and R. H. Hadfield, "Superconducting nanowire single-photon detectors: physics and applications," *Superconductor Science and Technology*, vol. 25, no. 6, p. 063001, 2012.

[98] A. D. O'Connell, M. Hofheinz, M. Ansmann, R. C. Bialczak, M. Lenander, E. Lucero, M. Neeley, D. Sank, H. Wang, M. Weides, J. Wenner, J. M. Martinis, and A. N. Cleland, "Quantum ground state and single-phonon control of a mechanical resonator," *Nature*, vol. 464, pp. 697–, Mar. 2010.

[99] P. M. Echternach, B. J. Pepper, T. Reck, and C. M. Bradford, "Single photon detection of 1.5 THz radiation with the quantum capacitance detector," *Nature Astronomy*, vol. 2, pp. 90–97, 2018.

[100] G. D. Mahan, "Thermionic refrigeration," *Journal of Applied Physics*, vol. 76, no. 7, pp. 4362–4366, 1994.

[101] D. G. Cahill, P. V. Braun, G. Chen, D. R. Clarke, S. Fan, K. E. Goodson, P. Keblinski, W. P. King, G. D. Mahan, A. Majumdar, H. J. Maris, S. R. Phillpot, E. Pop, and L. Shi, "Nanoscale thermal transport. ii. 2003–2012," *Applied Physics Reviews*, vol. 1, no. 1, p. 011305, 2014.

[102] N. Li, J. Ren, L. Wang, G. Zhang, P. Hänggi, and B. Li, "Colloquium: Phononics: Manipulating heat flow with electronic analogs and beyond," *Rev. Mod. Phys.*, vol. 84, pp. 1045–1066, Jul 2012.

[103] O. Quaranta, P. Spathis, F. Beltram, and F. Giazotto, "Cooling electrons from 1 to 0.4 k with v-based nanorefrigerators," *Applied Physics Letters*, vol. 98, no. 3, p. 032501, 2011.

Aalto-DD 216/2018

ISBN 978-952-60-8275-2 (printed)
ISBN 978-952-60-8276-9 (pdf)
ISSN 1799-4934 (printed)
ISSN 1799-4942 (pdf)

Aalto University
School of Science
Department of Applied Physics
www.aalto.fi

BUSINESS +
ECONOMY

ART +
DESIGN +
ARCHITECTURE

SCIENCE +
TECHNOLOGY

CROSSOVER

DOCTORAL
DISSERTATIONS